NASA CR-72231

NEUTRON FLUX DISTRIBUTIONS: (EXPERIMENT VS. THEORY) FOR A WATER REFLECTED SPHERICAL CAVITY SYSTEM

by

Floro Miraldi, George W. Nelson, Gary Holmberg and Gerald Skoff

CONTRACT NAS 3-6214

CASE INSTITUTE OF TECHNOLOGY

NOTICE

This report was prepared as an account of Government sponsored work. Neither the United States, nor the National Aeronautics and Space Administration (NASA), nor any person acting on behalf of NASA:

A.) Makes any warranty or representation, expressed or implied, with respect to the accuracy, completeness, or usefulness of the information contained in this report, or that the use of any information, apparatus, method, or process disclosed in this report may not infringe privately owned rights, or

B.) Assumes any liabilities with respect to the use of, or for damages resulting from the use of any information, apparatus, method or process desclosed in this report.

As used above, "person acting on behalf of NASA" includes any employee or contractor of NASA, or employee of such contractor, to the extent that such employee or contractor of NASA, or employee of such contractor prepares, disseminates, or provides access to, any information pursuant to his employment or contract with NASA, or his employment with such contractor.

Requests for copies of this report should be referred to

National Aeronautics and Space Administration
Office of Scientific and Technical Information
Attention: AFSS-A
Washington, D. C. 20546

NASA CR-72231

FINAL REPORT

NEUTRON FLUX DISTRIBUTIONS: (EXPERIMENT VS. THEORY) FOR A WATER REFLECTED-SPHERICAL CAVITY SYSTEM

by

Floro Miraldi, George W. Nelson, Gary Holmberg and Gerald Skoff

prepared for

NATIONAL AERONAUTICS AND SPACE ADMINISTRATION

December 31, 1966

CONTRACT NAS 3-6214

Technical Management
NASA Lewis Research Center
Cleveland, Ohio
Nuclear Reactor Division
Robert Hyland
Advance Systems Division
John C. Liwosz, Jr.

Case Institute of Technology
Cleveland, Ohio

NEUTRON FLUX DISTRIBUTIONS: (EXPERIMENT VS. THEORY)
FOR A WATER REFLECTED-SPHERICAL CAVITY SYSTEM

by

Floro Miraldi, George W. Nelson, Gary Holmberg and Gerald Skoff

ABSTRACT

Neutron flux distributions were measured in a system consisting of a large spherical cavity in water. Mathematical models were designed for the experiments and theoretical neutron flux distributions calculated. Three cavity geometries were studied including concentric sphere systems. Cavity fillings were air and BF_3 at various pressures between 0.05 and four atmospheres. Measurements were made by indium foil activation. Foil activation distributions are presented and relative thermal flux distributions are compared to calculated fluxes. Comparison of theory and experiment show good agreement.

SUMMARY

Experimental neutron flux distributions were measured in a water filled tank containing a 27-inch diameter spherical cavity region. Neutrons were provided by a plutonium-beryllium neutron source located at the center of the cavity, and bare and cadmium-covered indium foils were used to determine the neutron flux distributions in both the cavity and moderator regions. Three separate cavity systems were examined including the simple cavity, a concentric sphere system with a 9-inch diameter interior sphere, and a concentric sphere system with a 12-inch diameter interior sphere.

Foil activation distributions and thermal neutron flux distributions are presented for the several cavity geometries with cavity fillings of boron trifluoride gas to simulate a uranium gas-filled cavity. In the concentric sphere cases only the interior sphere was filled with boron trifluoride to simulate fuel contraction, and for these, various gas pressures were used to investigate the effects of varying absorption in the cavity.

The studies undertaken here are extensions of a previous study (1). In particular, BF_3 filling pressures in the simple cavity were extended to values below one atmosphere and in the concentric sphere systems, the pressures were increased to 4 atmospheres in the 9-inch interior sphere. The general features of the distributions are as expected and the flux peaking in the cavity, which was a distrubing feature of the previous study, is explained.

An extensive theoretical study of this system was undertaken

and the essential features of it are presented. Neutron flux distributions were calculated for the cavity system using a multigroup diffusion theory, the S_N method and an integral-age method. Agreement between the S_N procedure and experiment is very good.

It is shown in the study that calculations based on diffusion theory may be in error, and that in general, critical mass determinations by this method will be low. It is also shown that the neutron energy spectrum is hardened considerably as one progresses to the center of the cavity and that such spectrum changes must be considered in calculations of the neutron interaction rates in the cavity. The differences among the various theories are shown to be greatest for the systems with internal spheres where the absorbing gas concentrations are highest.

Finally, as an interesting aside, neutron lifetime measurements for two sphere systems are presented.

INTRODUCTION

In a previous report (1) a study of neutron diffusion in cavity media was described. Interest in such a study centered around the "cavity reactor" concept. This reactor system consists of a low density interior region surrounded by an external reflector-moderating region.

The previous study involved the measurement of the thermal neutron flux in a system composed of a large spherical cavity in water. Three separate systems were considered:

(1) Spherical cavity about 27 inches in diameter in water

(2) The same as (1) with a concentric 12 inch inner spherical cavity

(3) The same as (1) with a concentric 9 inch inner spherical cavity.

The particular experimental cases presented were:

(1) Single cavity with one atmosphere air filling

(2) Single cavity with one atmosphere BF_3 filling

(3) Concentric sphere system with 12 inch inner sphere and BF_3 fillings of 1, 2, and 2.5 atmospheres in the inner sphere

(4) Concentric sphere system with 9 inch inner sphere and BF_3 fillings of 1, 2, and 3 atmospheres in the inner sphere

(5) No cavity

The present report deals with the extension of these cavity experiments and the theoretical treatment of such systems. In particular, the experiments conducted were for low pressure BF_3 fillings in the simple cavity of 0.05, 0.1, 0.2 and 0.5 atmospheres; four atmospheres of BF_3 in the nine inch inner sphere system and three atmospheres of BF_3 in the 12 inch inner sphere system.

The theoretical treatment considers multigroup diffusion procedures, the S_N method, and combined integral-age method for the interior and exterior fluxes. The results agree well with the experiments and in addition yield interesting insight into the behavior of the neutron fluxes in these systems.

A separate set of experiments were conducted to measure the neutron lifetimes in two particular systems. These experiments were performed only for the purpose of investigating their feasibility. The results are presented but no theoretical treatment is given.

DESCRIPTION OF EQUIPMENT AND EXPERIMENTAL PROCEDURE

The Experimental Assembly

The equipment and precedures used in this work are essentially the same as the ones used in previously reported experiments (1), and therefore will not be presented in detail here. Only a summary is presented below for the convenience of the reader.

The experimental system consisted of a spherical cavity of 26-5/8 inch-diameter spun aluminum hemispheres welded together and containing either a concentric 12-inch-diameter internal sphere, a 9-inch-diameter internal sphere, or no internal sphere. This spherical cavity was anchored in the middle of a four-foot-diameter by four-foot-deep cylindrical tank of water. A 1-1/8 inch ID aluminum tube passed through the center of the spheres and through the sides of the water tank. A one-curie Pu-Be source was placed in this 'through-tube' at the center of the spheres. All irradiation of indium foils inside the cavity and some trial runs outside the cavity were done in this tube. Foils irradiated outside the cavity were also located in the water in plastic holders attached to a lucite rod. The trial runs showed the indium activation outside the cavity to be about 25 percent less in the through-tube compared with the corresponding in-water data. It was suspected that this was due to neutron streaming in the through-tube, and so all further irradiations outside the cavity were done in the water. Some unavoidable perturbations may have been introduced into the system by the presence of the through-tube. These perturbations are due to the presence of aluminum inside the sphere and the absence of BF_3 gas in the volume immediately surrounding the foils.

The indium foils, which were 1.20 cm in diameter and .005 inches

thick, were irradiated both bare and with .020-inch-thick cadmium covers.

Counting Procedure

The foils were counted with an Ohio-Nuclear Model III four-pi gas flow counter which used a counting gas of 90 percent argon and 10 percent methane. In the previous work reported (1), all data were taken as single 10 minute counts recorded on a RIDL Model 49-23 scaler. Such a procedure led to difficulties in separating the 54 minute activity from the 4-1/2 hour activity of indium. Accordingly, the counting procedure for the work reported herein was changed to a more accurate method.

In the present work counting was done with a TMC Model CN-110, 256 channel analyzer with a Model 214 multi-scaler plug-in unit. This system was set up to register consecutive 10 minute counts for several hours. The data were reduced by a computer program which made a least squares fit to the function $Ae^{-\lambda_1 t} + Be^{-\lambda_2 t} + C$, where λ_1 is the time decay constant of the 54-minute halflife of indium-116, λ_2 is the decay constant of the 4-1/2 hour excited state of indium-115 caused by inelastic scattering of fast neutrons from the source, and A, B and C are constants. The least squares program separately found the activity corrected for background of the 54-minute component and the 4-1/2 hour component at the end of irradiation.

EXPERIMENTAL RESULTS

This section presents the experimental results obtained for the various cases studied. These include

(1) Single cavity with BF_3 fillings of 0.05, 0.1, 0.2, 0.5 and 1.0 atmospheres pressure

(2) Concentric sphere system with 12 inch inner sphere and BF_3 filling of 3 atmospheres pressure in the inner sphere

(3) Concentric sphere system with 9 inch inner sphere and BF_3 filling of 4 atmospheres pressure in the inner sphere

(4) Neutron lifetime measurements (See Appendix A).

The results are presented in this section in tabular form only and are found in Table I. This section begins with some general comments about the results and follows with a discussion of particular cases. The section is concluded by a discussion of the data reduction procedures and the experimental precision.

General Comments

All data relative to these experiments (except lifetime measurements) are presented in Table I. The data presented are relative, 54 minute half-life, indium foil activations. These data are those directly related to the thermal neutron flux distributions.

The results for the interior regions were obtained in the through tube and the results for the exterior region were obtained by irradiating foils in the lucite holders* suspended in the water. The in-water data were obtained along two different radii. In one case the foils were placed along a line in the same vertical plane as the through-tube and inclined at an angle of 45° to it. In the

---

* This data will be referred to as in-water data in the following.

other case, the foils were along a radius in a plane normal to the through-tube and also inclined 45° to the horizontal plane. This choice of two different radial positions for in-water irradiations was unfortunate since it was later found that the neutron source was asymmetric. The in-water data thus has an additional spread; this point is discussed in the following sections.

It should be noted here that the activation data presented is in relative units and are consistant only for any one column in Table I. Through it was our aim to make the normalization for different cases always the same, a direct point by point comparison between columns is not recommended. To obtain a comparison between systems it is necessary to prepare graphs of the data in Table I and compare shapes. The comments made in the following are based on such comparisons.

Activation Profiles

Though the activation profiles differ greatly in the interior region for different systems, the activation in the exterior region a few inches from the sphere surface shows little change from one system to another. This is to be expected since the thermal flux deep in the water is closely related to the fast flux value at that point and the fast flux is not greatly affected by changes in the BF_3 filling.

Close to the source one observes an increase in the amount of scatter among data points. Although, one expects this region to have the least scatter, since the count rate is highest here, the 4-1/2 hour activity corrections are greatest near the source and the statistical errors from this relatively low activity are reflected

in the data.

In the single sphere system at 0.05 and 0.1 atmosphere BF_3 filling, rather significant drops in activity are observed at the interface. These are real and reproducible but are unexplained at this time. Measurements at higher pressure of BF_3, however, do not show this dip in surface flux. Since flux peaking in the water becomes significant at these higher pressures, it is probable that the flux suppression at the surface is compensated for by this peaking.

Data at distances of 0.5, 1.5 and 2.5 inches from the sphere surface in the water were found to be consistantly higher than expected in all sphere systems at all pressures. The cause is traced to the fact that these points were all taken along the radius in the plane perpendicular to the through-tube. A measurement of the anisotropy of the source revealed that the emission of the source in directions normal to the axis was about three percent higher than along the axis. Unfortunately, this measurement can not be applied directly to correct these activities since the thermal flux near the surface is a function of more than the source emission in the direction of the foil. There is little question, however, that the anisotropic nature of the source is the cause of the displacement of these points.

Since the effect of the anisotropy of the source is diminished as one proceeds deeper into the external region, the in-water data points along the two different radii become more convergent and their differences are quickly lost in the statistical counting errors. In obtaining the thermal flux from the activation data, a smooth curve is drawn through the data points and in this work, the data at 0.5,

1.5 and 2.5 inches from the sphere surface were neglected; though, in all cases these points are shown on the graphs. Hence, the profiles obtained here are those expected along the radius lying in the vertical plane of the through-tube and inclined at 45° to it. It is emphasized that the data is a function of the angular position of the foils relative to the axis of the source and therefore slightly different profiles will be obtained at different angles.

Flux Distributions

The relative neutron flux distributions were obtained from the activation data and are presented in the section on the "Comparison of Theory and Experiment" where the reader will find a description of the results as well as an explanation of some of the peculiarities observed.

The relative fast (epicadmium) flux is given by the cadmium-covered foil data. In Table I three separate cases are presented and one "average value" column is given. As can be seen, the differences between cases is small and for the count rates used, the differences are usually within one counting standard deviation. Accordingly, an "average" cadmium covered activity is presented. This average value was obtained by plotting all three cases on the same graph, passing the "best" smooth curve through the points, and using the curve value as the best representative of the data at a point.

The relative thermal flux was obtained as the difference of the bare foil data and the "average" cadmium covered data as presented in Table I after it is corrected for flux depression in resonance absorption by cadmium. The cadmium correction factor used was 1.07 and the flux depression correction factors used were 1.00 in the cavity region and 1.18 in the water

region. The choice of these particular correction factors is discussed in reference 1.

Reduction of Experimental Foil Data

Many simplifications were possible in this work since only relative data were needed. Additional reduction of the number of corrections needed were possible in many cases by employing certain experimental techniques such as using a constant count period and exposing the foils to saturation values.

The delay between the removal of the foil from irradiation to the start of counting was always at least 10 minutes so that all the 13 second half-life activity could be neglected. The foils were counted by an automatic system which made consecutive 10 minute counts for several to many hours. The data obtained were then reduced by a computer program which made a least squares fit to the function $Ae^{-\lambda_1 t} + Be^{-\lambda_2 t} + C$, where λ_1 is the time decay constant of the 54-minute half-life of indium-116, λ_2 is the decay constant of the 4-1/2 hour excited state of indium-115 caused by inelastic scattering of fast neutrons from the source, and A, B and C are constants. The least squares program found the initial activity of the 54-minute component at the time of removal, corrected for background and the 4-1/2 hour component; further corrections were made for foil weight, irradiation time, and detector normalization.

Counter resolving time corrections were not necessary because of the low count rates involved. Other corrections often employed, such as finite size source and detector corrections, were not considered appropriate for the presentation here and therefore were not applied.

Experimental Errors

It is extremely difficult to perform a rigorous error analysis of the data of this report; however, it is felt that such is not needed for this data to have meaning for the purposes considered here.

In general, for the bare foil data, the deviations of the data in the cavity region from a smooth curve through them is only a fraction of one percent; the maximum observed is about two percent. At the count rates used, the standard deviation is about one percent.

The same statistics were found for the in-water data. The discrepancies at 0.5, 1.5, and 2.5 inches from the surface of the sphere have already been discussed.

For the cadmium covered data, the deviations are considerably higher reaching a maximum of about eight percent but averaging about three percent. This is expected since the count rates were much lower and one standard deviation is about three percent.

Therefore it appears that throughout the experiment, the variations exhibited by the data can be attributed primarily to counting statistics.

Table I

Tabulation of Foil Activation Data

In the following tabulation relative, 54 minute half-life activities of irradiated indium foils are presented. Both bare and cadmium covered foil activities are given for the three systems investigated. Distances are measured from the cavity center. The cavity-water interface occurs at 13.31 inches from the center. This is denoted in the Table by a horizontal line above this point. The data above the horizontal line was taken in the through tube and the 13.537 inch point is actually beyond the cavity boundary.

Distance from center (inches)	Bare foils 0.05 atm BF_3 in no inner sphere system	Bare foils 0.1 atm BF_3 in no inner sphere system
1.037	1835	2016
1.537	2072	2043
2.037	2082	2111
2.537	2053	2136
3.037	2175	2076
4.037	2053	2106
5.037	2011	2131
7.037	2009	2084
9.037	1910	2112
11.037	2022	2078
12.037	1952	2066
13.037	1890	2005
13.537	1780	1973
13.31	1784	1967
13.81	1930	2068
14.31	1854	1980
14.81	1890	2089
15.31	1515	1797
15.81	1596	1819
16.31	1243	1463
17.31	802	1028
19.31	473	557
21.31	220	277
23.31	105	131
25.31	51	74
27.31	24	35

Distance from center (inches)	Bare foils 0.2 atm BF_3 in no inner sphere system	Bare foils 0.5 atm BF_3 in no inner sphere system
1.037	1691	1156
1.537	1696	1119
2.037	1787	1185
2.537	1761	1147
3.037	1769	1154
4.037	1769	1213
5.037	1774	1026
7.037	1749	1160
9.037	1729	1181
11.037	1733	1182
12.037	1712	1124
13.037	1704	1170
13.537	1702	1302
13.31	1659	1215
13.81	1847	1492
14.31	1902	1716
14.81	2019	1913
15.31	1707	1762
15.81	1789	1500
16.31	1504	1394
17.31	1088	1065
19.31	560	565
21.31	280	280
23.31	143	141
25.31	74	65
27.31	30	25

Distance from center (inches)	Bare foils 1 atm BF_3 in no inner sphere system
1.037	781
2.037	773
3.037	752
4.037	718
5.037	778
6.037	763
7.037	763
8.037	771
9.037	748
10.037	770
11.037	765
12.037	728
13.037	849
13.31	988
14.31	1619
15.31	1598
17.31	1044
18.31	745
19.31	554
20.31	368
21.31	278
22.31	169
23.31	135
24.31	97
25.31	64
26.31	34

Distance from center (inches)	Bare foils 4 atm BF_3 in 9" inner sphere system	Bare foils 3 atm BF_3 in 12" inner sphere system
1.037	1094	971
1.537	1151	927
2.037	1208	1015
2.537	1129	1025
3.037	1291	1047
4.037	1325	1086
5.037	1588	1209
6.037	1667	----
7.037	----	1436
8.037	1768	----
9.037	----	1450
10.037	1762	----
11.037	----	1453
12.037	----	1590
13.037	1734	1435
13.537	1705	1417
13.31	1716	1359
13.81	1736	1543
14.31	1634	1546
14.81	1702	----
15.31	1539	1479
15.81	----	1408
16.31	1211	1219
17.31	935	855
19.31	460	448
21.31	224	240
23.31	119	111
25.31	123	62
27.31	15	30

Distance from center (inches)	Cadmium covered foil activation for 9 inch inner sphere system	Cadmium covered foil activation for 12 inch inner sphere system
1.037	334	238
1.537	233	215
2.037	236	180
2.537	---	234
3.037	213	207
4.037	198	187
5.037	187	175
6.037	199	179
7.037	---	188
8.037	189	---
9.037	---	189
10.037	181	---
11.037	---	173
12.037	184	183
13.037	189	172
13.537	167	159
13.31	158	159
13.81	152	161
14.31	144	139
15.31	125	126
15.81	115	109
16.31	84	87
17.31	67	48
19.31	32	24
21.31	17	12
23.31	14	9
25.31	---	4

Distance from center (inches)	Cadmium covered foil activation for no inner sphere system	Average activation of cadmium covered foils
1.037	256	264
1.537	241	250
2.037	233	235
2.537	209	224
3.037	221	214
4.037	204	147
5.037	194	192
7.037	199	190
9.037	207	190
11.037	188	190
12.037	198	190
13.037	198	190
13.537	169	185
13.21	165	178
13.81	189	168
14.31	162	154
14.81	152	140
15.31	141	124
15.81	117	105
16.31	87	87
17.31	63	61
19.31	26	30
21.31	14	15
23.31	---	---
25.31	---	---
27.31	---	---

FLUX DISTRIBUTION CALCULATIONS *

Three standard approaches - multigroup diffusion, multigroup S_n and age-diffusion theory - are used to solve for flux distributions in the moderator. Of these, the multigroup diffusion and S_n theories also give a solution inside the cavity. The age solution is valid only in the moderator, so an integral transport method is used to calculate interior fluxes based upon exterior fluxes given by this theory.

For the multigroup approaches, selection of the proper cross section set is especially important for this system, because the source has an energy spectrum radically different from the fission spectrum, (see Figure 1) and because the system contains a large volume of nearly pure absorber which can cause considerable changes in the thermal neutron spectrum. Cross sections sets with 2, 3, and 16 groups were used in preliminary calculations, but these were inadequate to describe the Pu-Be source energy spectrum and the thermal spectrum changes in the BF_3 gas. A description of the cross section set used is presented in Appendix B.

---

* The contents of this section and the next two sections are presented in complete detail in "Thermal Neutron Flux Distributions in a Water System with an Internal Cavity," George W. Nelson, Ph.D. Thesis, Case Institute of Technology, November, 1966 (2)

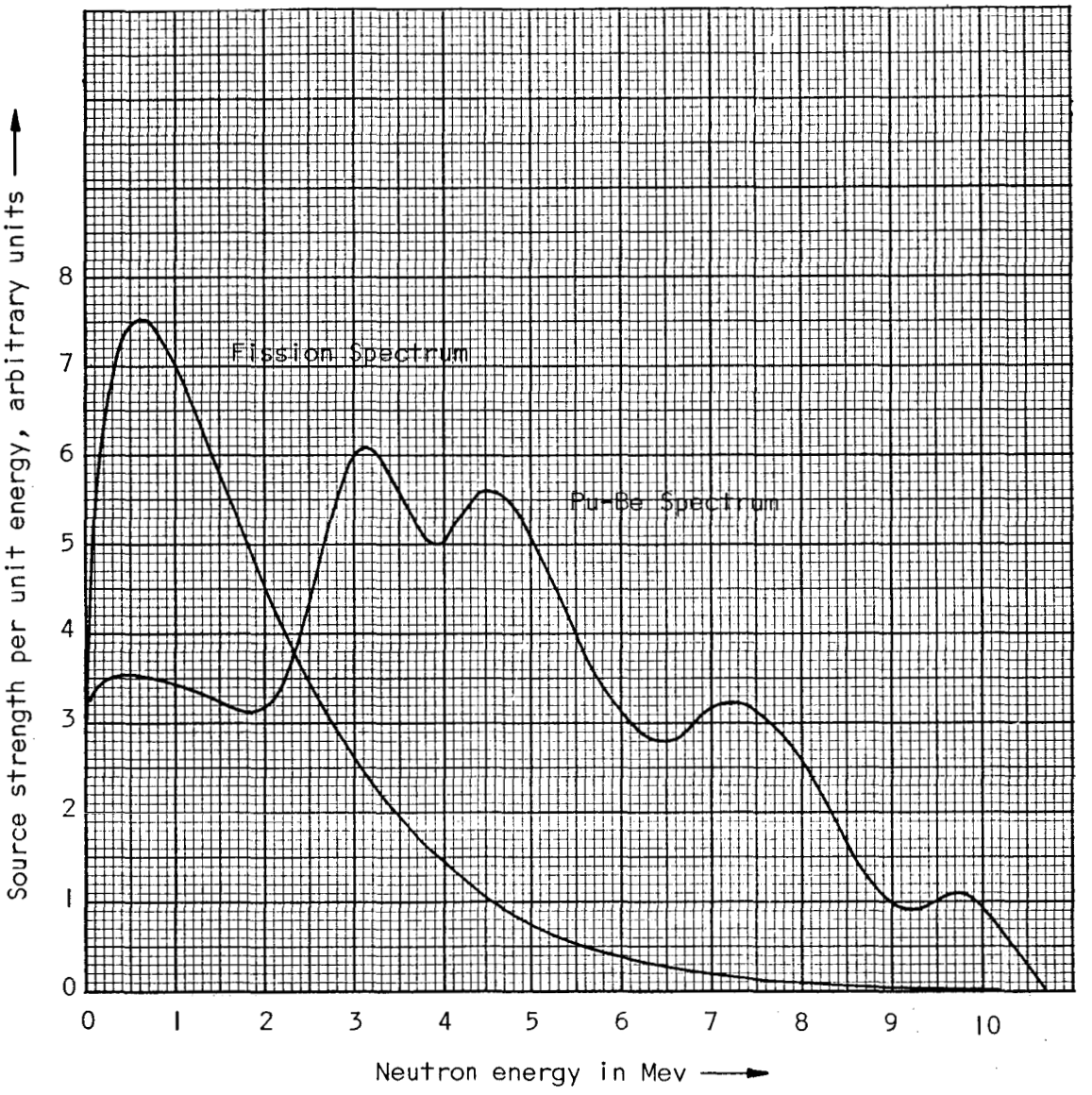

Figure 1. -- Comparison of fission spectrum [3] and plutonium-beryllium source spectrum [4].

Multigroup Diffusion

An evaluation of the neutron flux in the water given by ordinary multigroup diffusion theory was done by a central difference technique[5]. A derivation of the equations used in this computation and a discussion of the means used to speed up convergence of the computation is given in reference 2.

Since the validity of diffusion theory is questionable in regions where the atomic density is small, in media in which the absorption cross section is much greater than the scattering cross section, and near boundaries, the application of this procedure to the present cases leads to questionable results unless comparisons are made with a more rigorous theory or experiment. It is understandable, however, that because of the proven usefulness of diffusion theory in other situations, and because of the difficulties of using other procedures at the time that the NASA groups[6,7] and those at Douglas[8] did their work, that diffusion theory was used for critical studies. Accordingly, in this work a comparison of diffusion theory with those of other theories and experiments are included.

In order to simplify the comparison between the fluxes obtained by S_n and by diffusion computations, the same 26-group cross section set for water was used for both methods. The same scattering, transport, and absorption cross sections for the BF_3 gas and source metals were also used, but all scattering in these materials was assumed to leave neutrons in the same energy group. In the cross

section set used for the S_n computations, a small fraction of collisions, about .01 for the source metals and .001 for the BF_3 gas, resulted in neutron transfer to other energy groups. The source spectrum and system geometry were also identical to those used in the S_n computation.

The diffusion equations were solved analytically in the source, the gas, and the void regions, and the constants involved in this solution gave a boundary condition relating the flux at the cavity surface to the net current there. The solution in the water was then made by an iterative central difference method.

The same outer boundary condition was used for the multigroup diffusion computations as was used in the S_n computation -- that is, no return current from the outer boundary of the system. The following boundary conditions were used to evaluate the flux inside the cavity and to get the boundary conditions for the water computation.

(1) Flux finite at the origin.

(2) Φ source $(R_s) = \phi$ gas (R_s), where R_s is the outer boundary of the source.

(3) $-D$ source $\nabla\Phi$ source $= -D$ gas $\nabla\Phi$ gas $+ f_i/4\pi R_s^2$ at R_s, where f_i is the fraction of source neutrons in group i.

(4) Φ gas $(R_1) = \Phi$ water (R_0), which equates the flux at the inner sphere surface, R_1, to the flux at the outer sphere surface, R_0.

(5) $-4\pi R_0^2$ D water $\nabla\Phi$ water $(R_0) = -4\pi R_1^2 D$ gas $\nabla\Phi$ gas (R_1), equating the net current out of the water to the net current into the inner sphere.

The S_n Method

The S_n solutions for this system were run on Argonne National Laboratory's CDC 3600 computer, using a discrete ordinate S_n code called SNARG ID[9], which is modeled after the S_n code DTF. Both of these codes are based upon the S_n discrete ordinate method developed by Bengt G. Carlson at Los Alamos to solve the neutron transport equation[10,11].

Considerable literature has been written on the subject of the mathematical model used in S_n codes[12,13] and the reader is referred to the references.

It was found that to solve a problem containing 70 space points in the S_4 approximation with a 26-group cross section set, 9 groups of which contain upscattering, about 70 outer iterations are required to bring about convergence with a convergence factor of .0001. The total computing time per problem is thus about one hour. However, the number of outer iterations needed to obtain convergence could be greatly reduced when a good initial flux guess was used as input to the problem. In order to obtain such a good initial guess, the fluxes were first computed using a cross section set for water with no upscattering, which required only one outer iteration and about four minutes of computing time. The cross sections were obtained by removing the upscattering from the water by the formulae

$$\sigma^{\text{no upscatter}}_{i\to j} = \frac{\sigma^{\text{upscatter}}_{i\to j}\,\Phi_i - \sigma^{\text{upscatter}}_{j\to i}\,\Phi_j}{\Phi_i} \qquad i<j \qquad (1)$$

$$\sigma^{\text{no upscatter}}_{j\to i} = 0 \qquad i<j \qquad (2)$$

The Φ_i are typical water fluxes from one problem with zero atmospheres of BF_3 which was allowed to run to completion at 70 outer iterations with upscattering present. With this input flux guess, convergence was usually obtained after about 10 outer iterations with the upscattering cross section set.

One S_{16} calculation was done, and the flux shapes were not found to differ significantly from an S_4 calculation of the same problem. It was concluded that an S_4 calculation is sufficiently accurate for calculating flux shapes; this was fortuituous, since the iteration time required per problem is roughly proportional to the S_n order.

For all of the S_n calculations, a reflective boundary condition was used at the origin. Incoming currents were taken as zero at the outside boundary of the system. An isotropic source was distributed throughout the source volume at the center of the sphere. The source spectrum, which was based upon an integration of the experimental Pu-Be spectrum of Anderson and Bond [4], covered the nine highest energy groups.

A description of the system upon which calculations were performed is given in Table 2, along with a description of the actual experimental system.

TABLE 2

DESCRIPTION OF THE EXPERIMENTAL AND CALCULATED SYSTEMS

Description of the Experimental System	Description of the Calculated System (S_n)
Outer sphere radius 33.8 cm	Outer sphere radius 33.8 cm
Inner sphere radius 11.43 or 15.24 cm	Inner sphere radius 11.43 or 15.24 cm
Water blanket - a cylinder of radius 60.9 cm, height 121.8 cm	Water blanket - a sphere of radius 60.9 cm
Absorbing gas - boron trifluoride	Absorbing gas - boron trifluoride
Space between inner and outer spheres filled with one atmosphere dry air	Space between inner and outer spheres is a void
Source metals in the shape of a cylinder of radius 1.35 cm and height 3.11 cm	Source metals in the shape of a sphere of radius 1.765 cm (equivalent volume)
Source metals are concentric cylindrical shells of stainless steel and tantalum containing a core of Pu-Be alloy	Source metals homogenized
Source spectrum Pu-Be	Source spectrum is Pu-Be spectrum of Anderson integrated into group structure

Fermi Age

This method makes use of a derivation originally done by Wallace and LeCaine[14] for a point source in a non-absorbing spherical cavity surrounded by an infinite moderator. It was extended by Safonov to apply to a cavity completely filled with a homogeneous absorbing medium. Safonov states that the flux exterior to such an absorbing cavity can be described by the relation

$$\Phi(r,\tau) = \Phi_v(r) - \left\{\frac{\gamma\,\Phi_v(a)}{\gamma\,\Phi_p(a) - D\,\nabla\Phi_p(a)}\right\}\Phi_p(r) \qquad (3)$$

moderator

where a is the cavity radius, Φ_v is the Wallace and LeCaine solution for the cavity with no absorption, and Φ_p is the flux for a point source of neutrons in the moderator with no cavity. Φ_v and Φ_p are functions only of the thermal diffusion properties of the moderator, the age of the neutron source to thermal, and the radius of the cavity. γ is called the 'interior greyness' and is defined by the relation

$$\gamma = \frac{\text{Net current into the interior}}{\text{Flux at interior boundary}} \qquad (4)$$

The techniques used here are simply the evaluation of Safonov's equation with two modifications.

Safonov uses a single Fermi age in his calculations. This is not strictly correct except for a monoenergetic source of neutrons, but for the fission spectrum (see Figure 1) it gives a good answer. This is not so for the Pu-Be spectrum, and so in the calculations done here

the energy spectrum was broken up into several groups, and an average age to thermal was calculated for each group. Then the flux due to the entire Pu-Be energy spectrum was calculated as the sum of the fluxes due to each group source weighted by the fraction of the spectrum in that group, i.e.

$$\Phi(r) = \sum_i f_i \, \Phi(r,\tau_i) \qquad (5)$$

This summation is possible because there are no interactions between neutrons originating in different age groups.

This principle is illustrated in Figure 2, where the fluxes $\Phi(r,\tau_i)$ from each of eight age groups are shown individually, together with the summed flux for the whole spectrum.

A second modification was necessary so that the method could apply to a problem with a void, internal concentric spheres, and a source. This was done by an iterative integral transport method for evaluating γ for the more complicated interior. In the iteration, an initial value for γ was used to calculate the Fermi age flux in the water. With this flux the integral transport method was used to calculate the net current and flux at the cavity surface, the ratio of which gave a new γ. This new γ was again used to calculate a Fermi age flux. When two successive values of γ differed by less than one part in 10^{-5}, the iteration was stopped and the Fermi age fluxes printed out.

Since γ is a slowly varying function of the initial flux shape, convergence comes quickly; a typical problem converges in 3 or 4 iterations with an initial guess for γ which is 20 percent high or

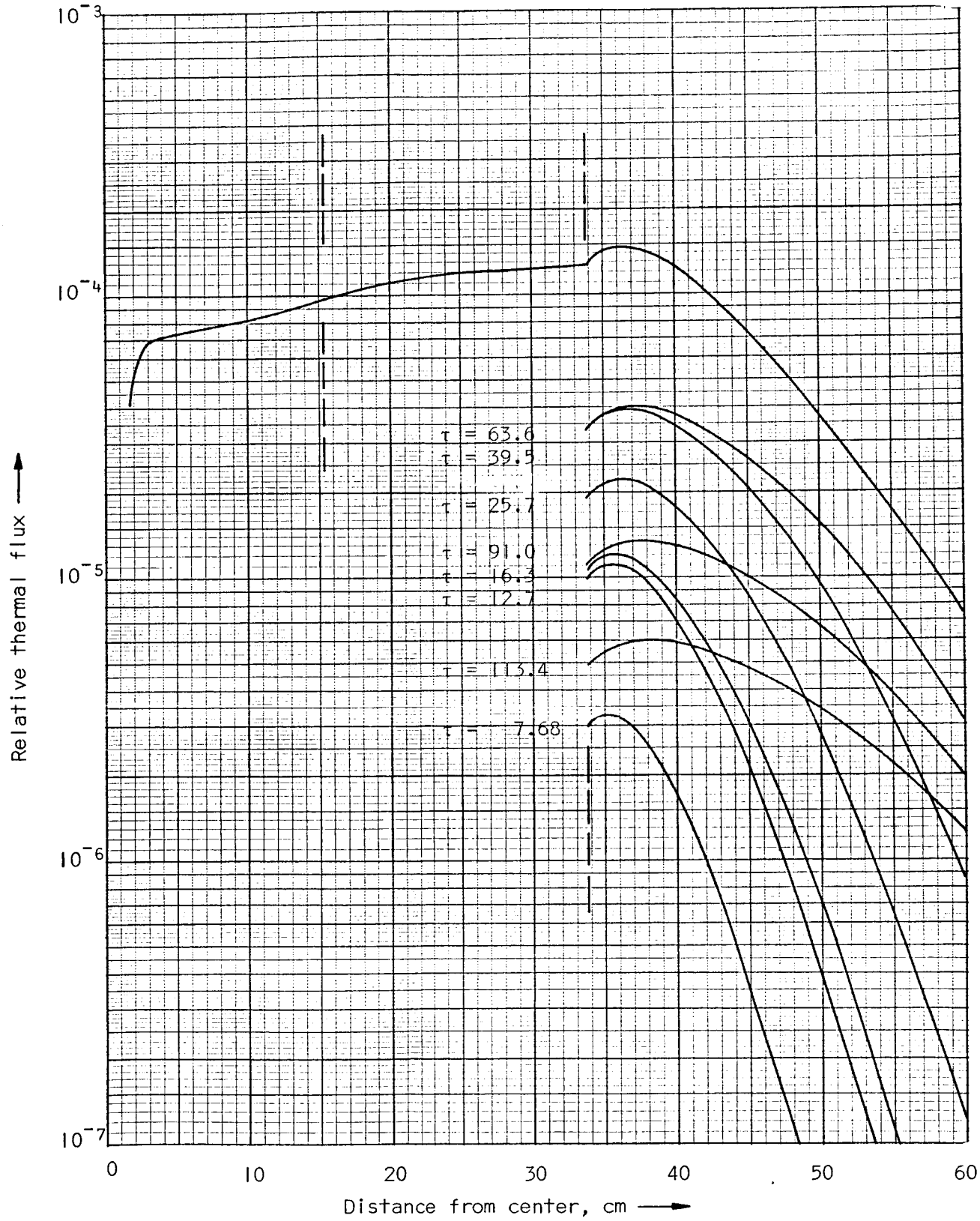

Figure 2. -- Lower curves: individual group fluxes in the water from eight age groups for the 12-inch internal sphere system with 2.0 atmospheres BF_3 filling. Upper curve: the Pu-Be spectrum flux, which is the sum of the lower curves.

low. The validity of this method is demonstrated by the fact that γ's calculated for the no-inner-sphere case by this method agree with those calculated from Safonov's results to within one percent.

The thermal diffusion parameters for ordinary water which were used in the Fermi age calculations are the often-quoted values of 2.72 cm for the diffusion length and .164 for the diffusion coefficient. These yield Σ_a of water of .022 cm^{-1} and Σ_{tr} of 2.032 cm^{-1}. The boron absorption cross section used in the calculation was the Maxwellian average at 293°K based on the 2200 m/s value of 755 barns. τ_i^{in}, the average age to the 1.457 ev indium resonance for group i, and f_i, the fraction of the source spectrum in group i, were evaluated by numerical integration of the functions

$$\tau_i^{in} = \frac{\int_{E_{Li}}^{E_{Hi}} \tau(E)\ F(E)dE}{\int_{E_{Li}}^{E_{Hi}} F(E)dE} \qquad (6)$$

$$\text{and} \quad f_i = \frac{\int_{E_{Li}}^{E_{Hi}} F(E)dE}{\int_{0}^{\infty} F(E)dE} \qquad (7)$$

where $\tau(E)$ is the age to indium resonance as generated by the CHRONOS Monte Carlo code [15], and $F(E)$ is the Pu-Be spectrum of Anderson and Bond [4]. The age to thermal, rather than the age to indium resonance, is used in the calculation, and so the age from

indium resonance to thermal of 1.0 cm was added to each of the $\tau_i^{in_{16}}$.

Formulae for Φ_p and Φ_v for finite spherical systems are also included in the report by Wallace and LeCaine[14]; these functions could be used in Safonov's equation instead of the ones for infinite media. However, the solution done here could use the simpler infinite medium solutions because the minimum surrounding thickness of moderator is 27.1 cm, and this is effectively an infinite medium for light water.

*It is interesting to note that if one performs the summation

$$\bar{\tau}^{in} = \sum_i f_i \tau_i^{in}$$

one gets the answer $\bar{\tau}^{in} = 53.5\ cm^2$, which is in good agreement with the experimental value of $\tau_{in} = 52.8 \pm 2.5\ cm^2$ reported by Valente and Sullivan[17].

Integral Transport Method of Finding the Interior Flux

If the neutron distribution in the moderator is known, then this distribution can be used to calculate a source term for those neutrons passing through the cavity. That is to say, each small volume element of moderator is considered to be a point source of neutrons. The strength of this source is equal to the scattering per unit volume at the point times the dV volume element. One can then calculate the fraction of neutrons from that point which pass through any part of the interior. In this case it was assumed that there is only absorption and no scattering in the interior. In this method, the source term, modified by the geometric attenuation and the exponential attenuation passing through moderator and gas, is integrated over the volume of the moderator. This yields a rather complicated double integral for the interior flux and currents which is solved by numerical integration. Derivations of the integrals for two systems are presented in reference [2]; the first is the simplest case of a sphere uniformly filled with absorbing gas and surrounded by moderator; the second is the most complex system which consists of five regions: (1) moderator, (2) a thin, absorbing shell (aluminum or deposited boron), (3) a void, (4) absorbing gas, and (5) an absorbing central sphere to mock up the absorption of the source metals. Any one of the regions in the latter system can be eliminated to make a simpler system. For example, the width of the void region can be made zero in order to give the no-inner-sphere case.

The accuracy of this method depends primarily upon how well one knows the flux in the moderator, and upon the assumption of no scattering inside the sphere. The assumption that there is no thermal scattering in the source metals is valid since the source is small and located at the origin; neutrons scattering from the source would give almost the same neutron distribution as neutrons passing through the source. Furthermore, the absorption cross section of the source metals is about four times as great as the scattering cross section, so most of the neutrons which enter the source are absorbed there.

The assumption of no scattering within the sphere is not basic to the method, but if scattering is allowed within the sphere, the source of neutrons passing through the sphere is also inside the sphere itself, and so two changes are necessary: (1) the integration must extend over all scattering sources, so it must include the whole sphere, and not just the moderator, and (2) repeated iterations are needed since sources in the sphere are calculated by the preceeding integration.

Such a procedure was not necessary in this case since for .025 ev neutrons the scattering cross section of BF_3 gas is only 16 barns, compared to 755 barns for the absorption cross section.

This internal integral method was used to find the interior flux for all calculations which used the modified Fermi age method for the exterior flux. The source of thermal neutrons was calculated as the product of the scattering cross section, the flux, and the volume element.

$$q(r) = \Sigma_s^{th} \Phi(r)^{th} dV \qquad (8)$$

This integral procedure could also be used to solve for interior fluxes using outside fluxes calculated by a multigroup approach. In this case, the interior flux would be calculated for each group, and the source for any group i would be calculated as the sum

$$q_i(r) = \Sigma_{j \to i} \Phi_j(r) dV \qquad (9)$$

where $\Sigma_{i \to j}$ is the product of the macroscopic cross section for scattering times the probability that a neutron in group j will change energy on scattering enough to be in group i.

The method can also be adapted to give the parameter γ which is defined by equation (4) for a given flux distribution. This was done in the calculations in which the exterior flux was calculated by the age method.

COMPARISON OF RESULTS

Figures 3 through 15 show thermal flux distributions for three sphere geometries determined by the following four methods:

(1) 26-group S_n calculations -- the thermal flux was chosen to be the sum of the fluxes in groups 19 through 26.

(2) 26-group diffusion calculations -- thermal flux chosen to be the sum of the fluxes in groups 19 through 26.

(3) An age calculation of the exterior fluxes coupled with an integral transport method for the interior fluxes.

(4) Experimental thermal flux distributions derived from indium foil activations.

The quantity which is plotted as thermal flux for the S_n and multigroup diffusion computations is the sum of the computed fluxes in groups 19 through 26, which are the eight lowest energy groups of the 26-group set. These groups cover an energy range from .001 to .2 ev. It is difficult to say exactly what the upper energy cutoff for thermal energies should be, but this was chosen because the Maxwellian distribution for room temperature neutrons drops off sharply at .2 ev. At any rate, whether the highest thermal energy is chosen to include groups 18, 19, or 20 makes little difference in the thermal flux graphs, since only a relatively small part of the thermal flux is in these groups.

Figure 3 shows a comparison of the magnitude of thermal flux found by the three analytical methods. The curves show the resultant thermal neutron flux from a unit neutron source. The flux found by the diffusion theory method is significantly greater than either that

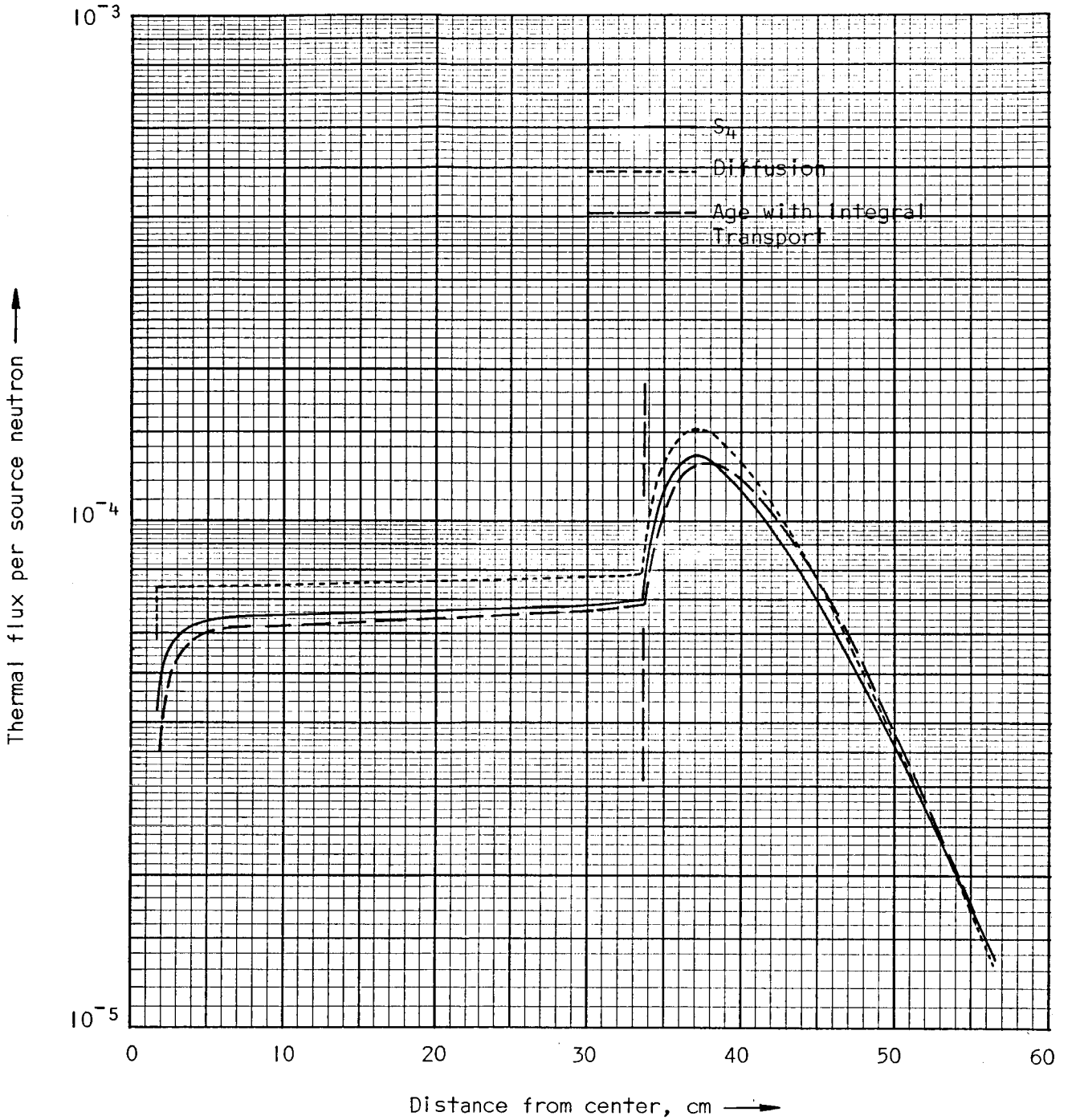

Figure 3. -- Comparison of the relative magnitude of fluxes calculated by the three analytical methods for the single sphere system with 0.5 atmosphere BF_3 filling.

found by S_n or age theory. Since the diffusion theory calculation uses the same absorption cross sections in the cavity, it can be concluded that a lower critical mass would be found by diffusion theory for this type of system.

In the rest of the figures the theoretical fluxes are individually normalized to best fit the experimental thermal flux data points at the surface of the outer sphere.

In Figures 4 and 5, all three analytical methods seem to give a good agreement with the experimental fluxes from the two single sphere cases with BF_3 fillings. In Figure 6, which is the single sphere case with no BF_3 filling, the age calculation gives fluxes in the water which are almost 10 percent higher than those found either by experiment or by the S_n method. This does not necessarily prove that the age treatment does not work well for this system for two reasons: (1) Because of asymmetry of the source emission and also because of a possibility that the flux depression factor used to correct the experimental data in the water may be low, it is possible that the experimental flux in the water should be higher. The effect of source asymmetry is discussed in Appendix C. (2) Since the age method does not use the same high energy water cross sections as the S_n method, a direct comparison between the two methods is difficult. Some of the difference shown in Figure 6 may not be due to the method, but rather to the use of different input data to calculate the parameters describing the fast neutron penetration in the water.

Except for normalization, there appears to be a close similarity

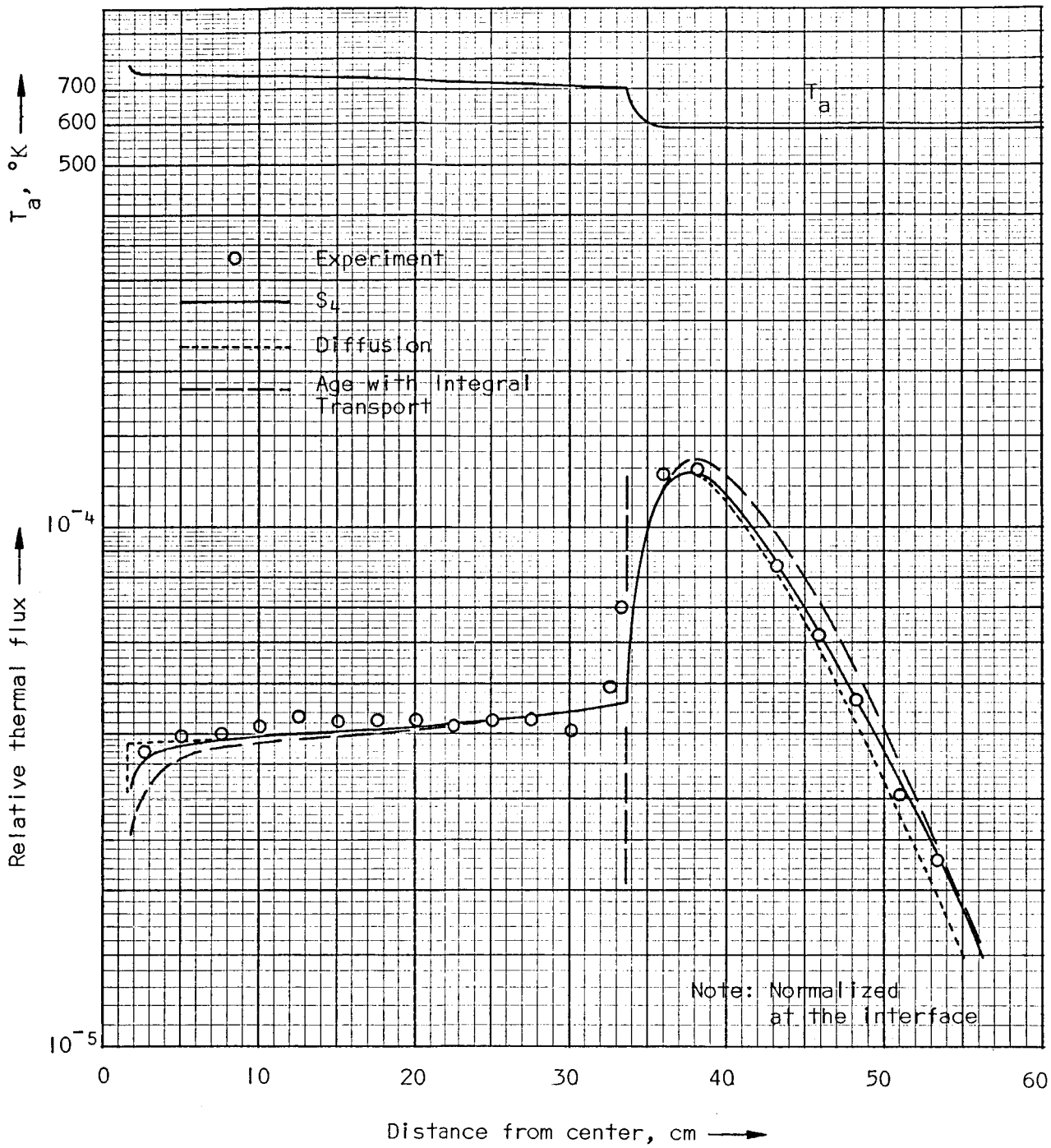

Figure 4. -- Comparison of calculated and experimental flux distributions for the single sphere system with 1.0 atmosphere BF_3 filling.

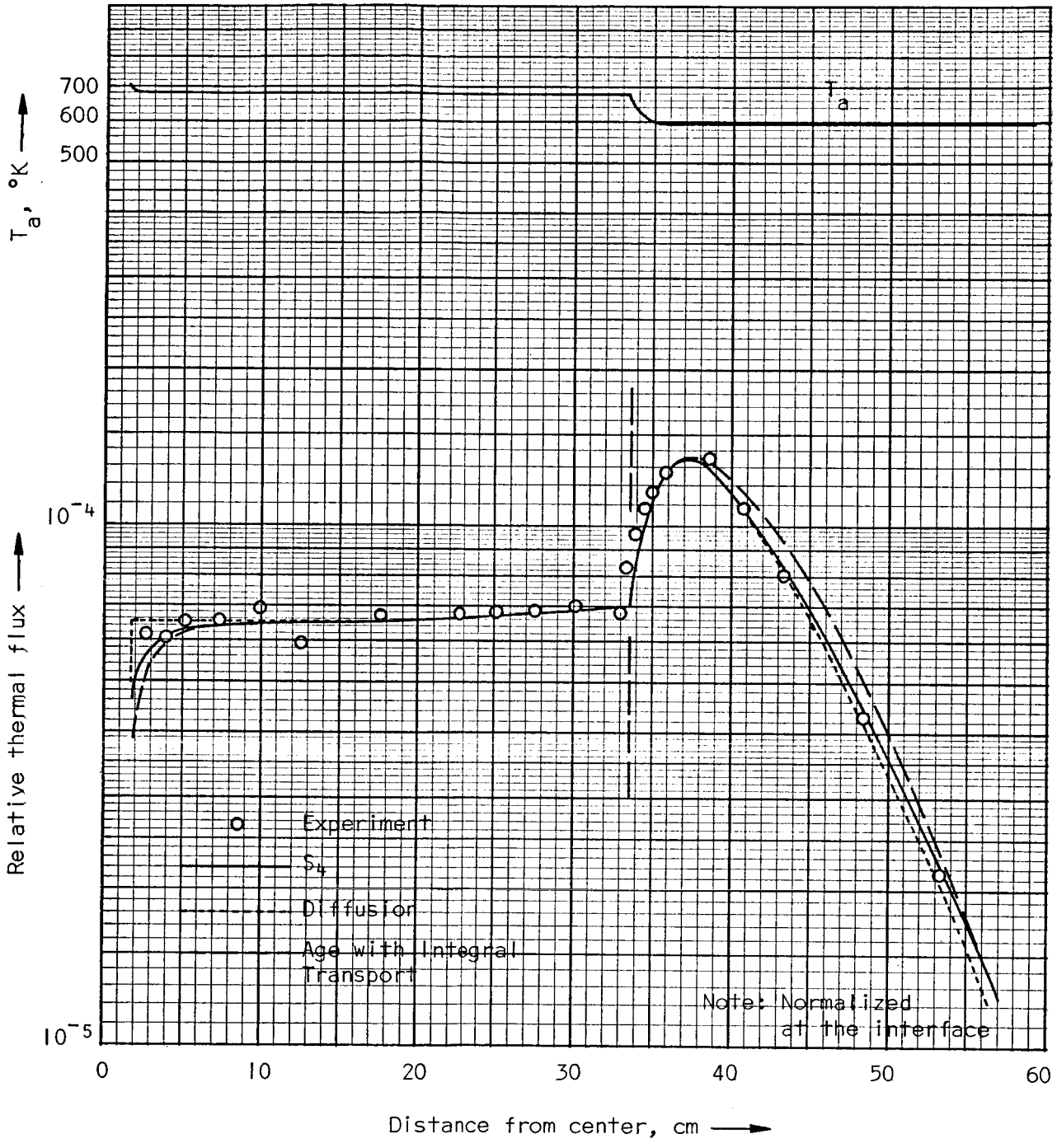

Figure 5. -- Comparison of calculated and experimental flux distributions for the single sphere system with 0.5 atmosphere BF_3 filling.

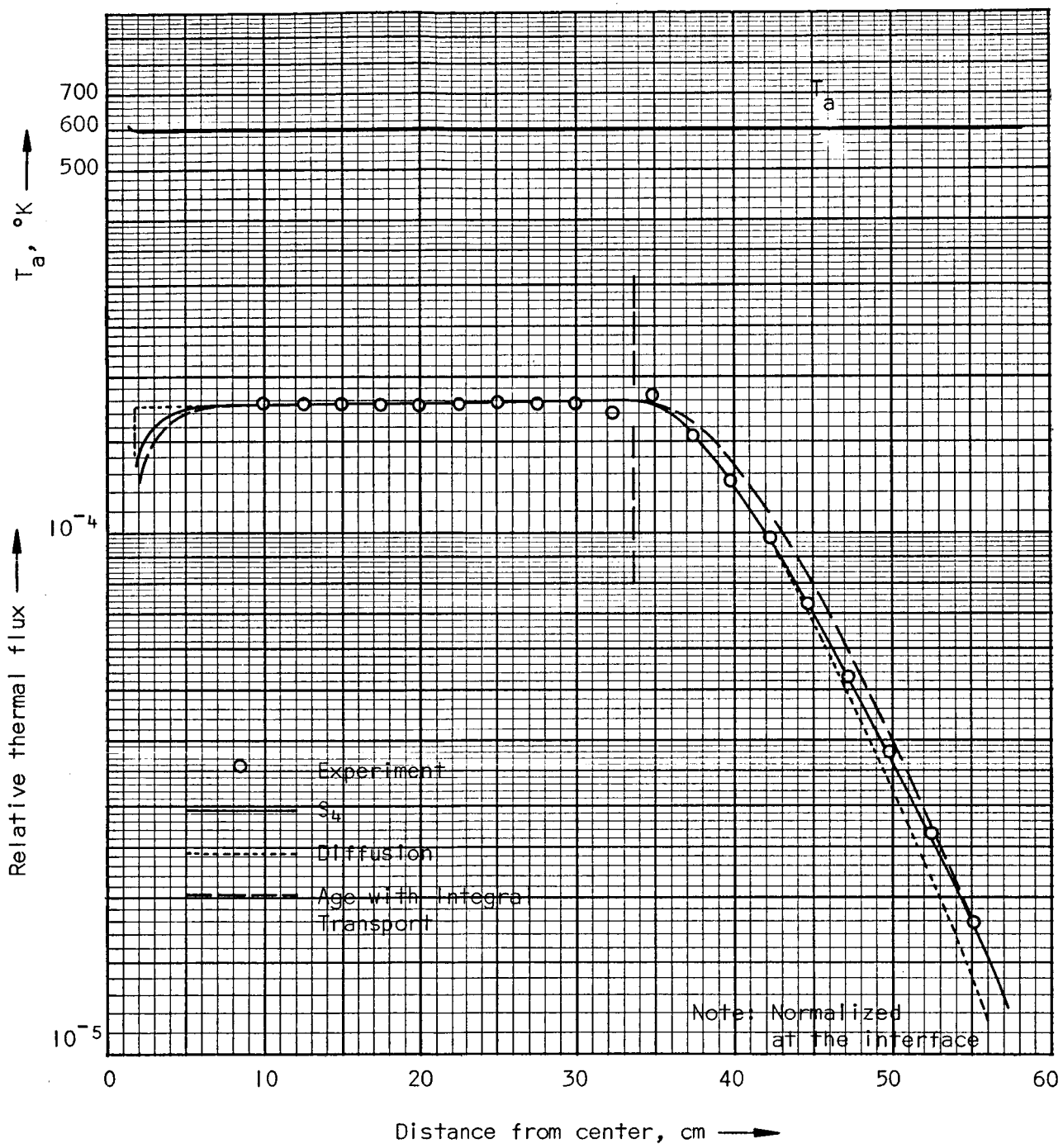

Figure 6. -- Comparison of calculated and experimental flux distributions for the single sphere system with no BF_3 filling.

between the S_n and multigroup diffusion results for the system with no internal sphere. This agrees in part with the findings of Plunkett and Holl[8], who found agreement between S_n and diffusion calculations for systems both with and without internal spheres. Unlike the results of Plunkett and Holl, however, a considerable difference was found between the S_n and diffusion theory fluxes for internal sphere systems in this case. This can be seen in Figures 7 through 10. These results are so different from the other two analytical methods that a check was made on the multigroup diffusion calculation procedure by performing calculations using the cross section sets and system geometry used by Plunkett and Holl for two graphite-U^{235} systems. The agreement with their flux distributions (Figures 3.1 and 3.2 in SM-44041) both with and without an inner sphere was perfect, as it should be*. Assuming their S_n calculations are also correct, it becomes obvious that the conclusions made by Plunkett and Holl regarding the similarity of results from the two methods is true only for their particular system.

Ragsdale and Hyland[6] qualify their use of diffusion theory by referring to a statement by Safonov that diffusion theory is adequate if the interior greyness, γ, (defined by equation (4) of this thesis) is less than 1/3. The results pictured in Figures 7 through

*The fact that the flux distributions were identical confirms the validity of the assumption which was made in deriving the analytical diffusion solution for the interior -- that there is no significant energy transfer in the scattering of neutrons in the gaseous core.

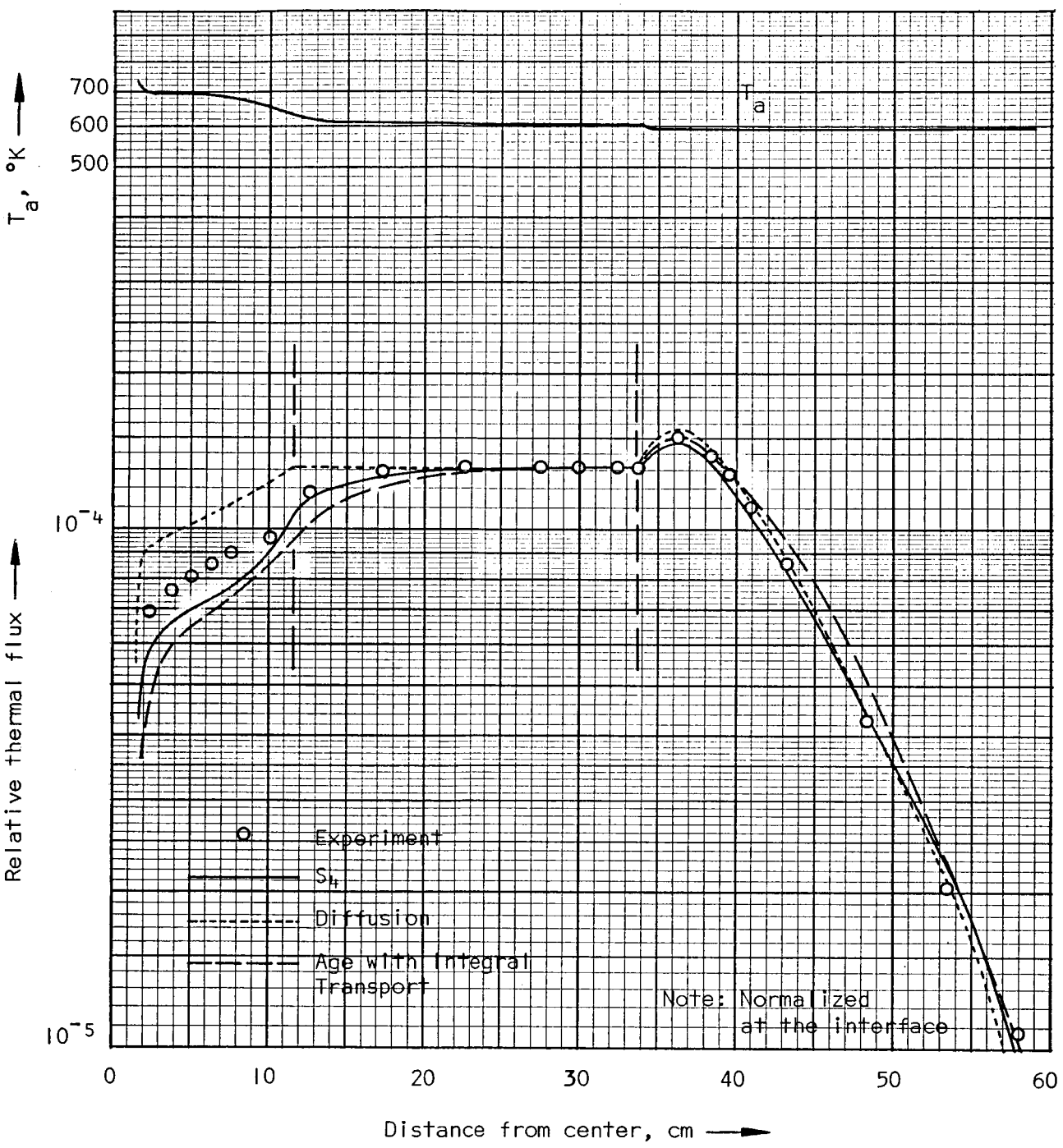

Figure 7. -- Comparison of calculated and experimental flux distributions for the 9-inch inner sphere system with 4.0 atmospheres BF_3 filling.

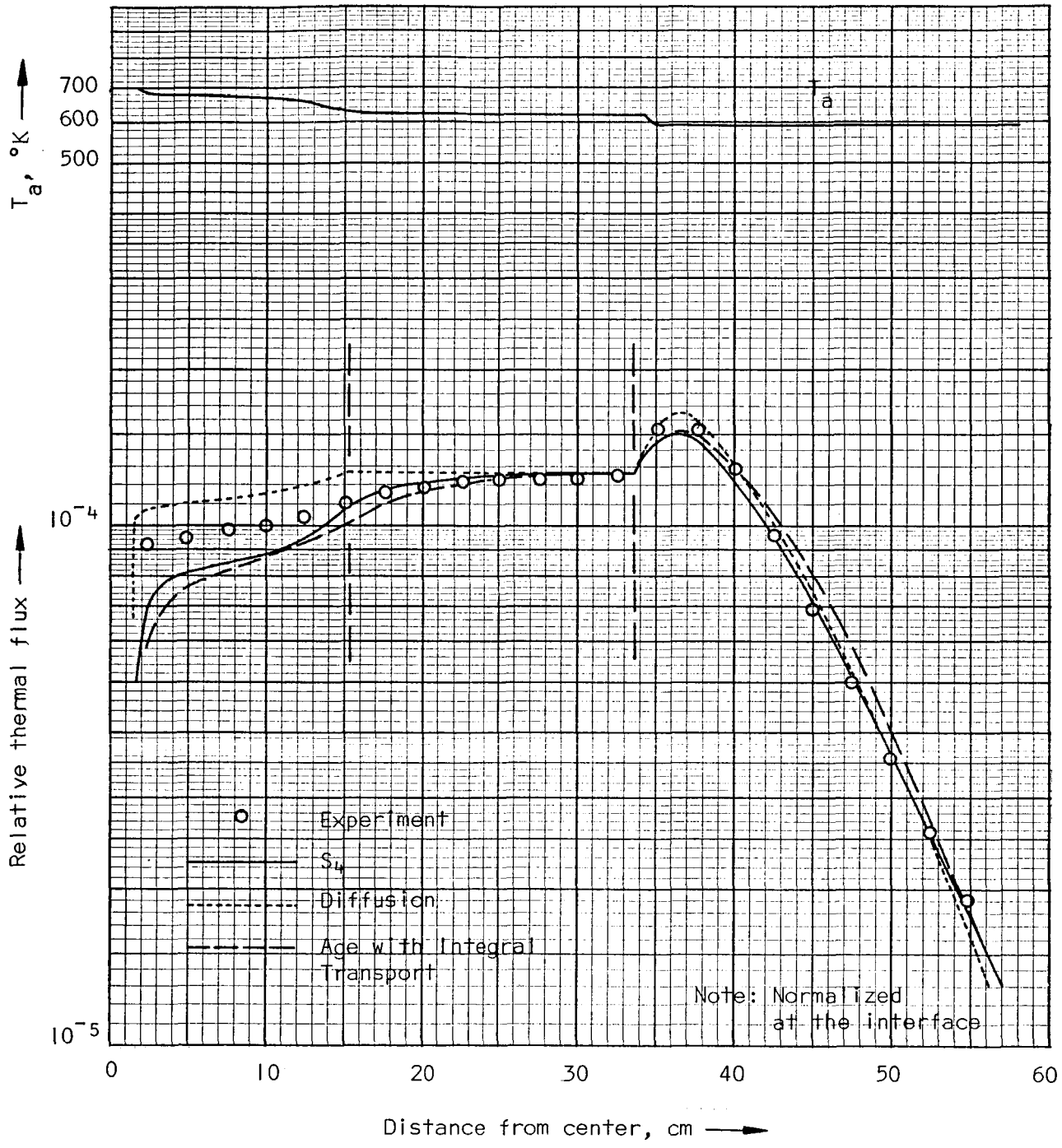

Figure 8. -- Comparison of calculated and experimental flux distributions for the 12-inch inner sphere system with 2.0 atmospheres BF_3 filling.

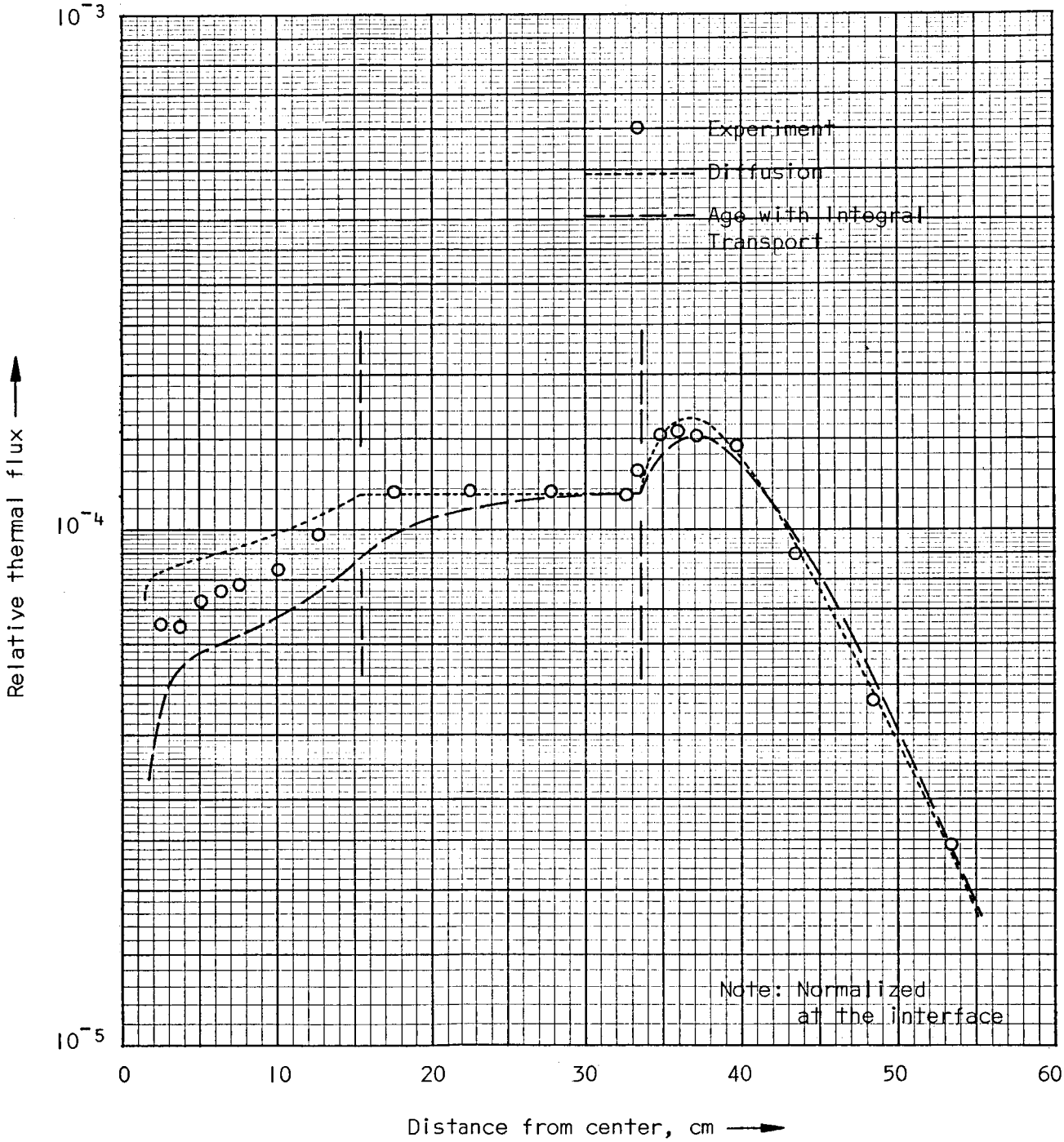

Figure 9. -- Comparison of calculated and experimental flux distributions for the 12-inch inner sphere system with 3.0 atmospheres BF_3 filling.

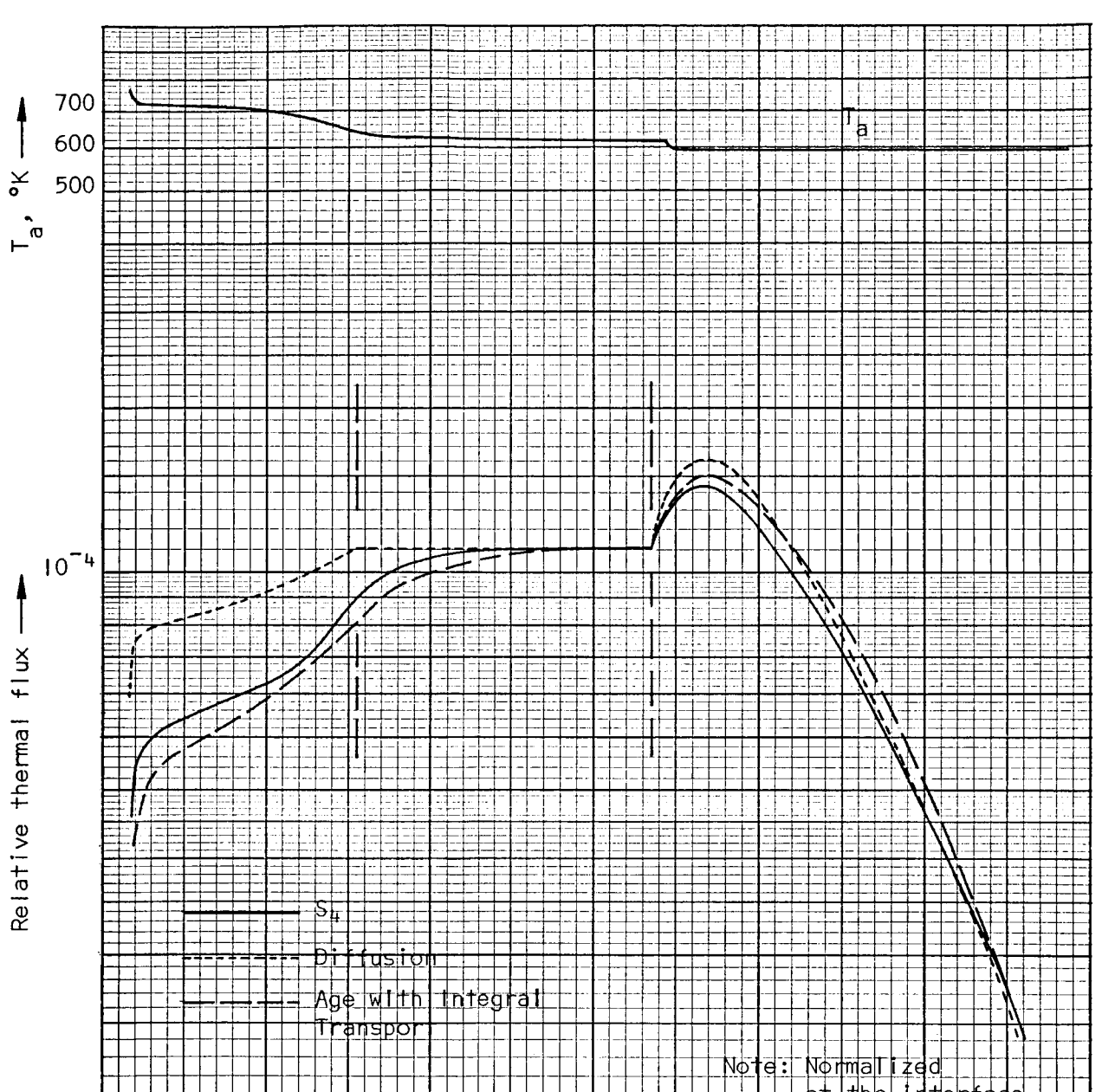

Figure 10. -- Comparison of the calculated fluxes for the 12-inch inner sphere system with 3.5 atmospheres BF_3 filling.

10 show that this is not an adequate criterion. The Plunkett and Holl graphite-U^{235} inner-sphere system calculated here had a maximum γ of .1115, while the water-BF_3 system pictured in Figure 10 had a maximum γ of only .09773. Safonov's criterion indicates that the water-BF_3 system is more nearly correct, and this is certainly not true. Furthermore in the most extreme case of one atmosphere of BF_3 in the no-inner-sphere system, γ had a value of .4268, which is significantly above 1/3, yet the agreement with the S_n calculation is good (see Figure 4). Obviously a more valid criterion for the use of diffusion theory is needed. Since Plunkett and Holl made comparisons with the more rigorous S_8 method over the whole range of geometry and cross sections which their calculations covered, they are justified in their use of diffusion theory. The conclusion of this comparison is that workers in the field who use diffusion theory should make comparisons with a rigorous theory or with experiment.

Calculated and experimental thermal fluxes for the two internal sphere systems are compared in Figures 7 through 10. Both S_n and age-integral transport agree with experiment in the water and in the void, but are significantly less inside the BF_3 core. It is likely that the experimental fluxes are incorrect here because of neutron streaming in the through-tube. The outer diameter of this tube is 1-1/4 inches and the radii of the two internal sphere systems are 4-1/2 and 6 inches. Since many of the neutrons which are absorbed in a foil enter the foil from a direction nearly perpendicular to the flat foil surfaces, a significant fraction of such neutrons will have passed

through the air in the tube rather than through the BF_3 gas in this case. Another cause of the experimental flux being too large is that the difference in thermal neutron spectra between the void and cavity was not taken into account to correct for self shielding in the foil. The effect of this cause is probably much less than the former, however.

The integral transport calculation agrees fairly well with the S_4 results inside the cavity, except for showing a lower flux and thus greater absorption in the gas. This is probably because the boron absorption cross section used in the integral transport calculations was the Maxwellian average at the moderator temperature. This is identical to the way most previous workers have calculated cavity absorption cross sections, and it is not correct. As will be discussed in detail in the following pages, spectrum hardening in the presence of the absorbing gas causes the actual absorption cross section to be considerably less.

Figures 11, 12, and 13 are composite curves of the three sphere systems at all BF_3 filling pressures for which experimental activations were measured. The experimental points are not included, but the comparison of experiment to theory for these figures follows the same pattern observed in Figures 4 through 10, where there is good agreement at all points in the single sphere system, but only in the void and moderator in the systems with internal spheres.

Figures 14 and 15 show the effect of having one atmosphere of BF_3 evenly deposited on the interface instead of being in gaseous form

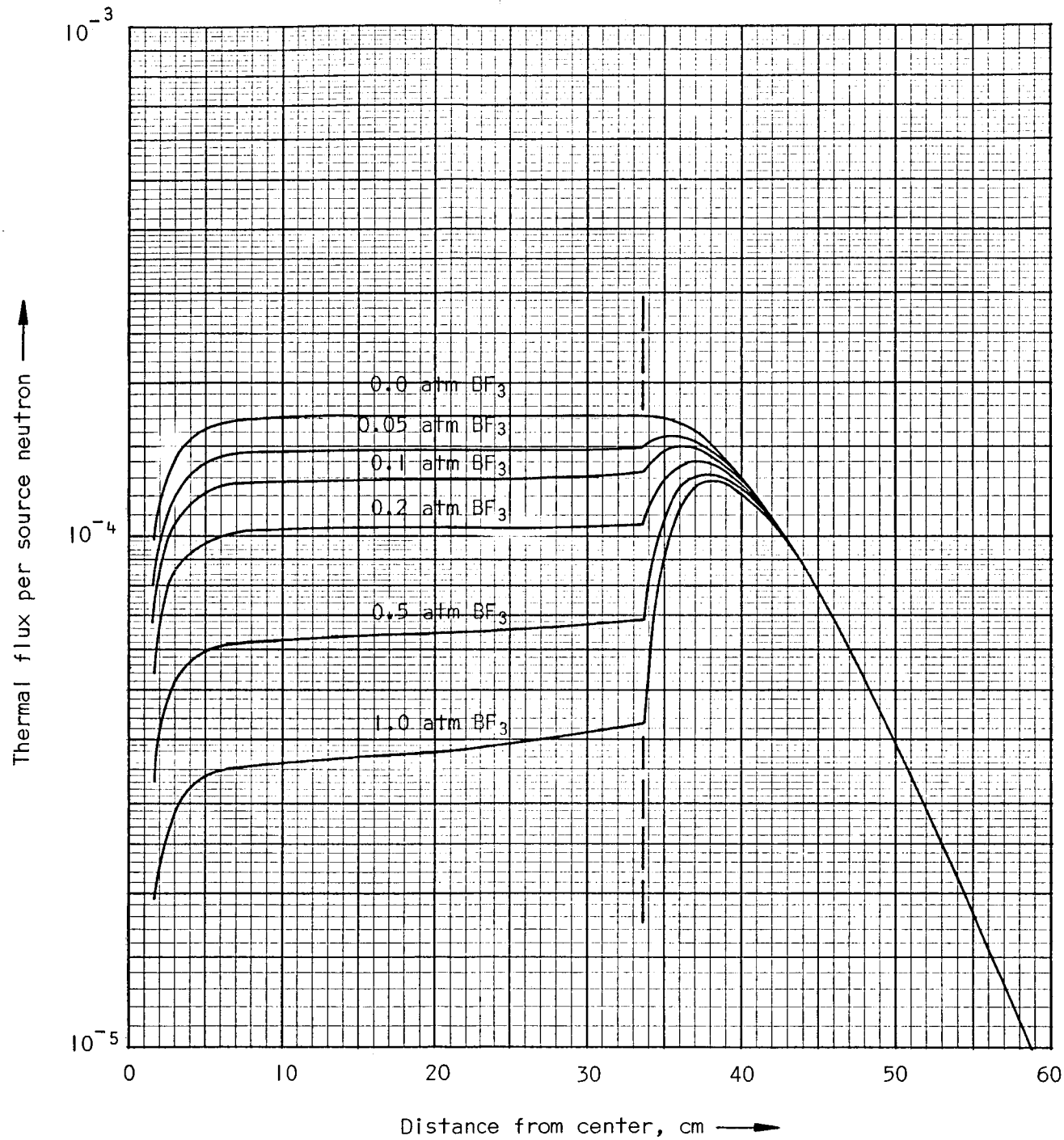

Figure 11. -- Theoretical thermal fluxes calculated by the age-integral transport method for the single sphere system with various BF_3 filling pressures.

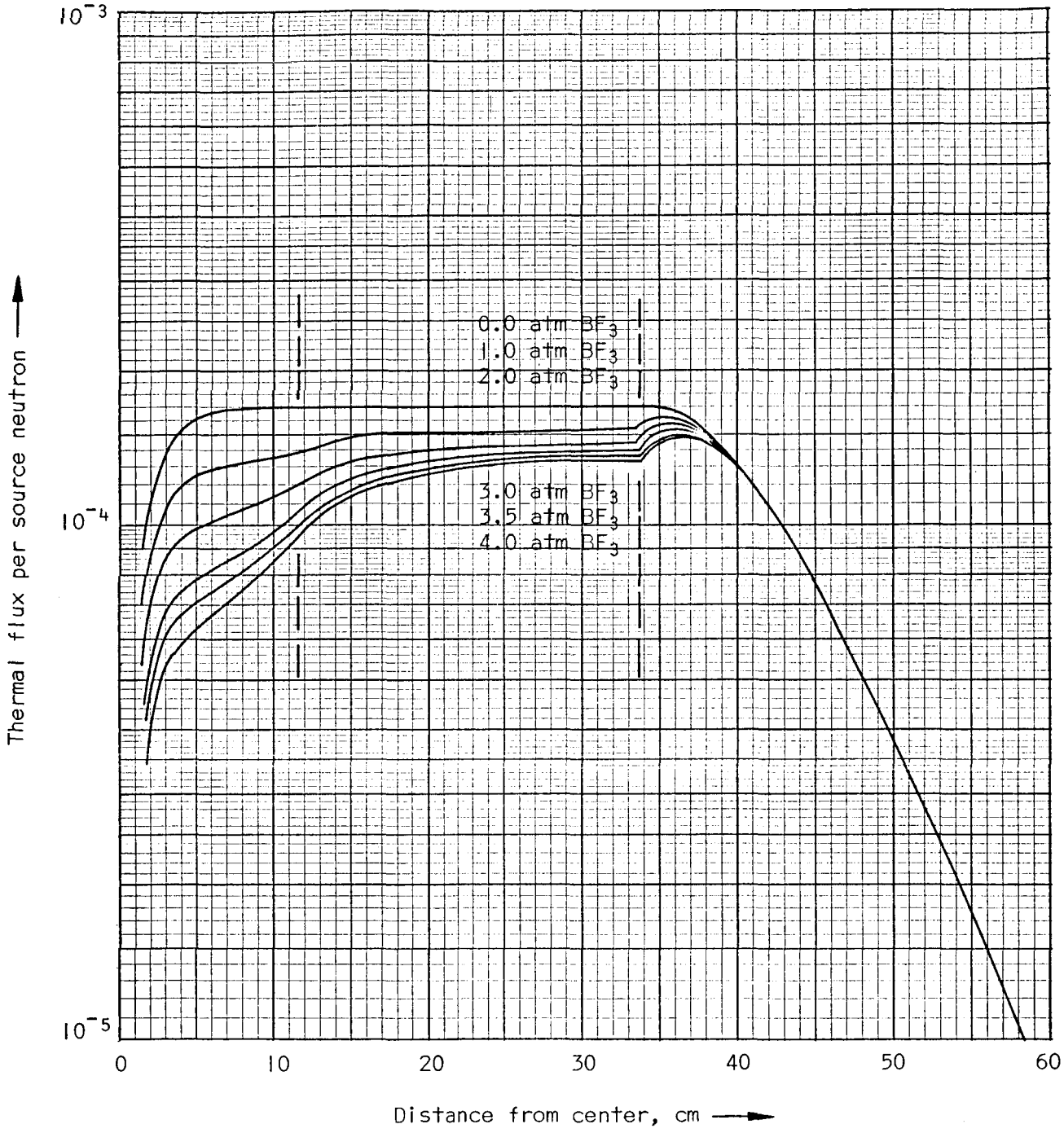

Figure 12. -- Theoretical thermal fluxes calculated by the age-integral transport method for the 9-inch internal sphere system with various BF_3 filling pressures.

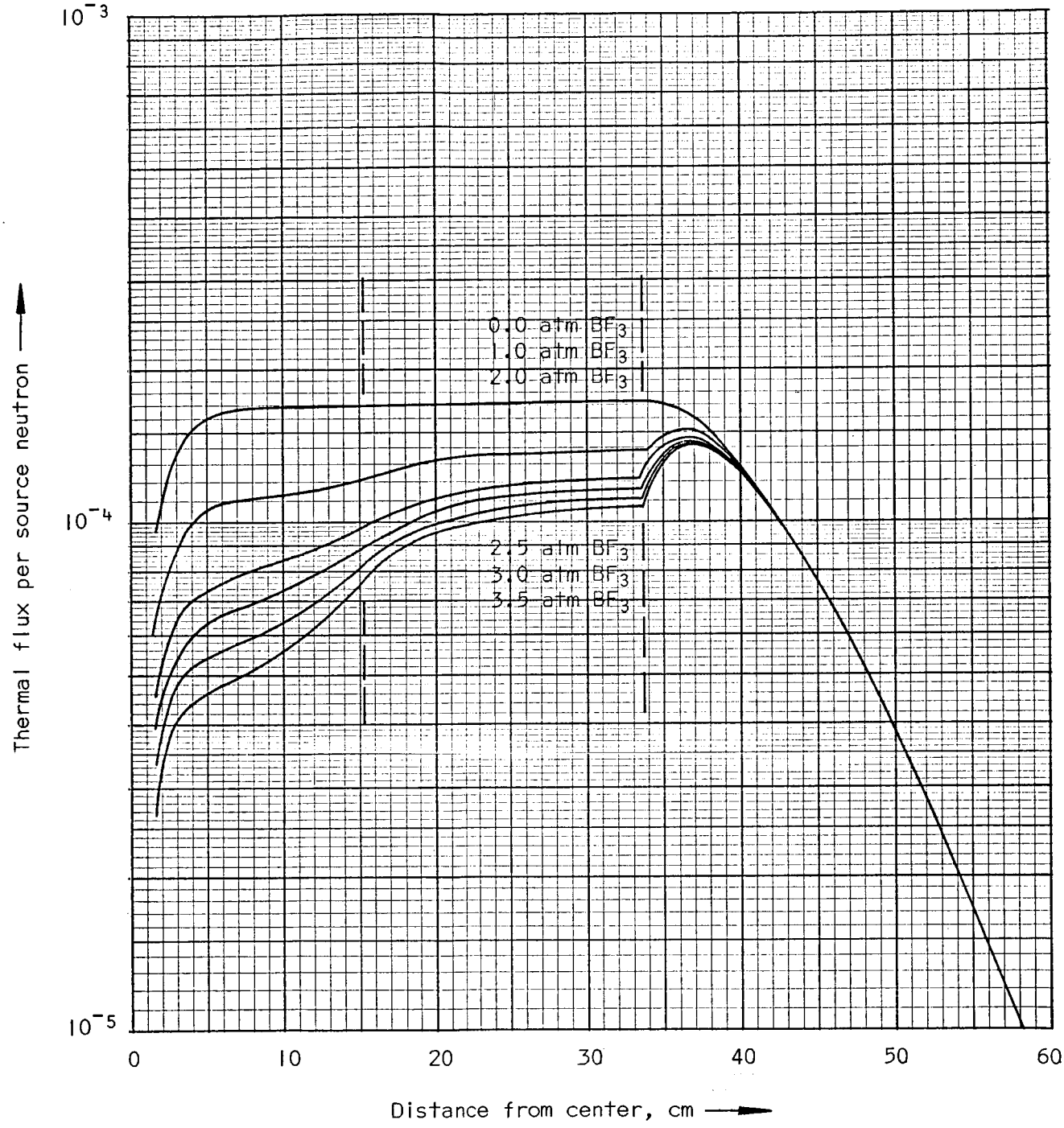

Figure 13. -- Theoretical thermal fluxes calculated by the age-integral transport method for the 12-inch internal sphere system with various BF_3 filling pressures.

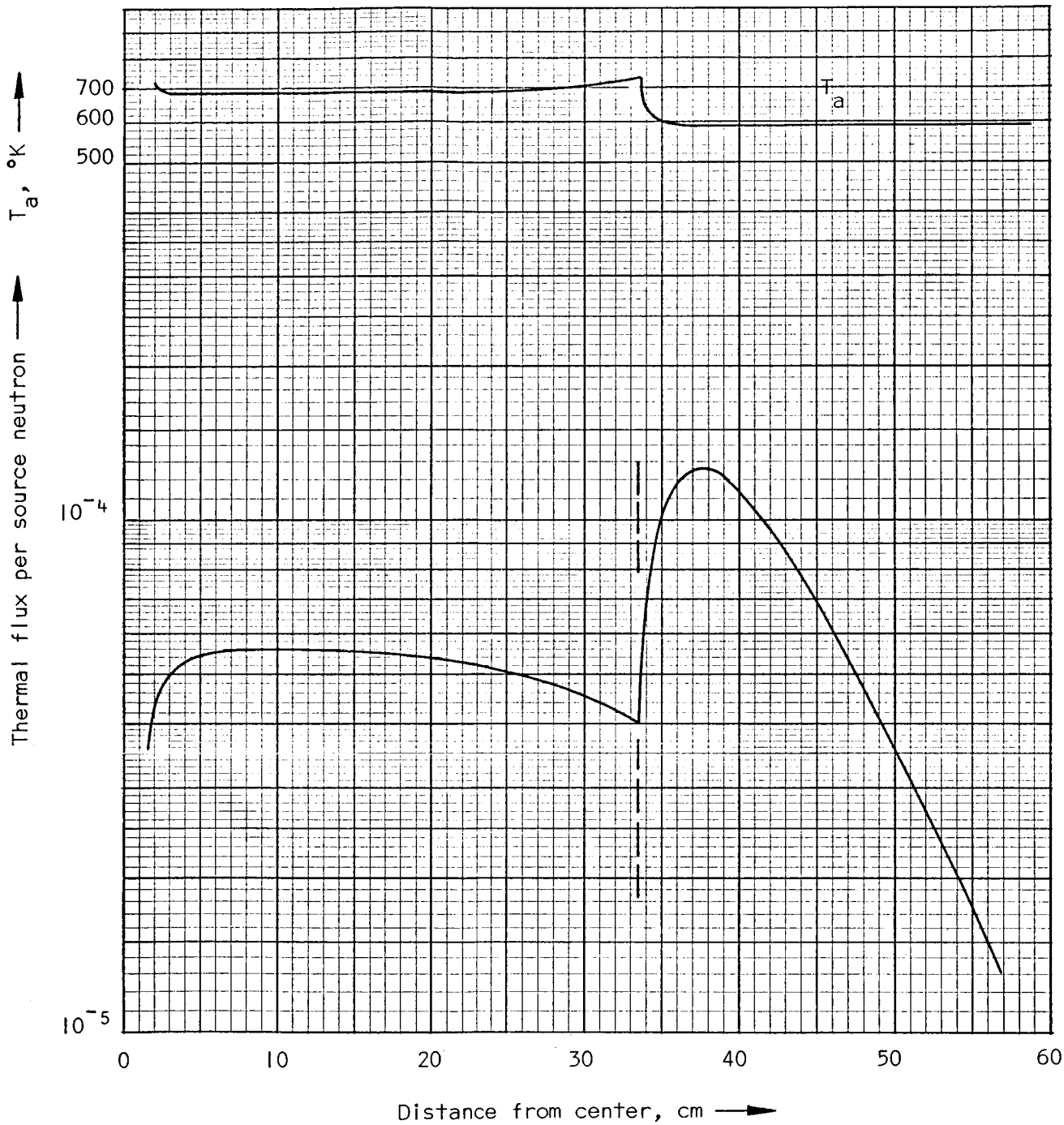

Figure 14. -- S_4 calculation of the thermal flux distribution which results when all of the BF_3 from 1.0 atmosphere filling in the single sphere system is deposited on the interface.

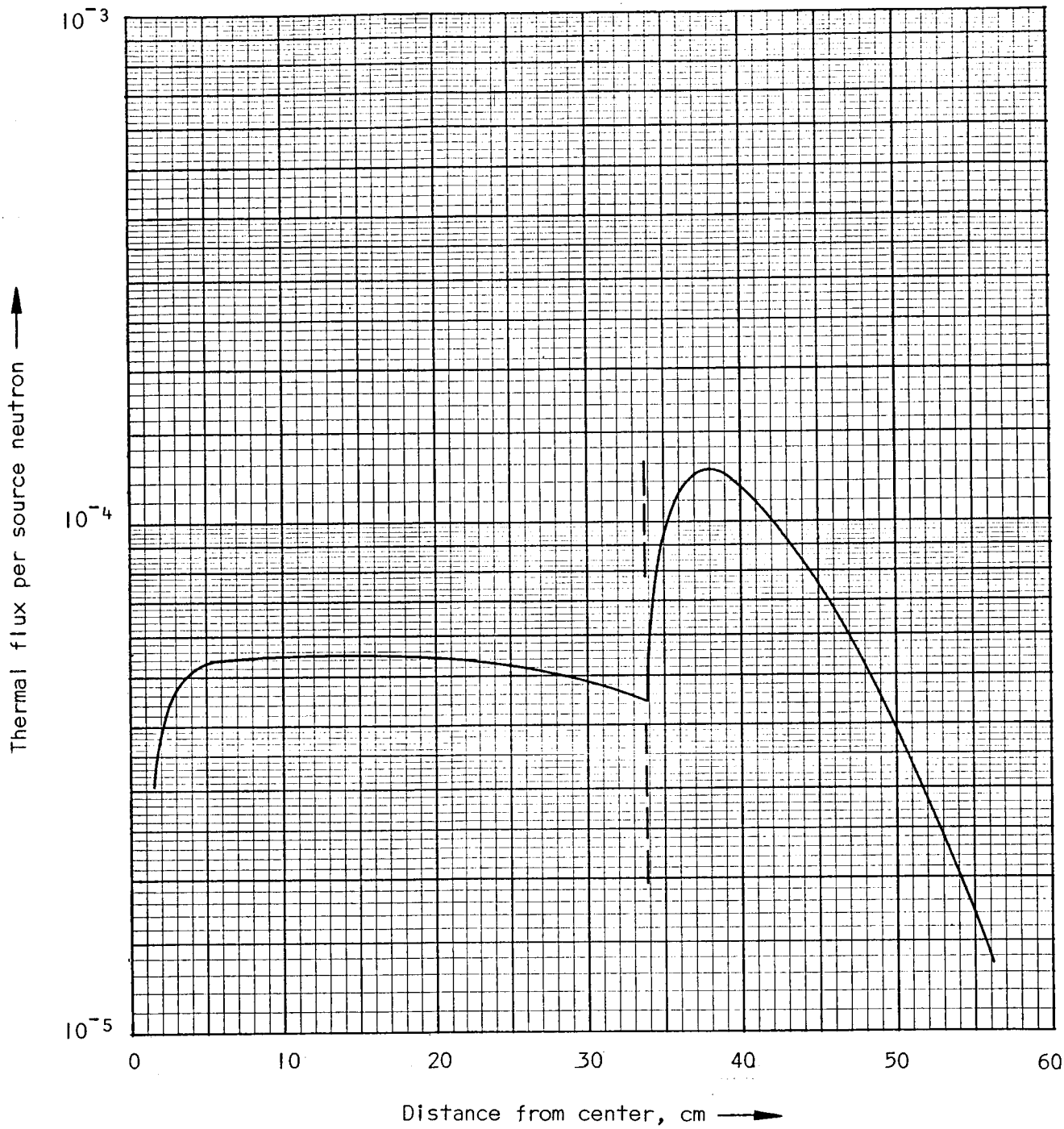

Figure 15. -- Age-integral transport calculation of the thermal flux distribution which results when all of the BF_3 from 1.0 atmosphere filling in the single sphere system is deposited on the interface.

inside the cavity. These calculations are included since it is suspected that some boron may have been deposited on the inside of the outer sphere, and that this may have been a cause of the peaking phenomenon. These figures show that such a deposit will result in peaking. Unfortunately the inside surface of the sphere was not tested for boron deposits after the experiments, so the magnitude of this effect in the experimental data is open to conjecture.

The relative fluxes in the low energy groups give an idea of the thermal spectrum and the way it varies within the system. Figure 16 shows a typical flux spectrum histogram in the water from the S_n computation, with the experimental spectrum of Poole superimposed. It appears to agree well with Poole's data. A Maxwellian distribution of neutron energies with $T_{effective}$ equal to 291°K gives a good fit to Poole's data except above .2 ev, where the Maxwellian has a sharp drop-off with higher energy, while Poole's spectrum has a 1/E tail.

One way of showing how the spectrum varies between different parts of the system is to calculate the average temperature of the thermal neutrons from the multigroup fluxes. This has been done with the S_n results, and the average temperatures are labelled T_a on Figures 4 through 10. This average spectrum temperature was calculated be weighting the average neutron temperature of each group by the fraction of the flux in that group using the formula

$$T_a = \frac{\sum_{i=19}^{26} \Phi_i T_a^i}{\sum_{i=19}^{26} \Phi_i} \qquad (10)$$

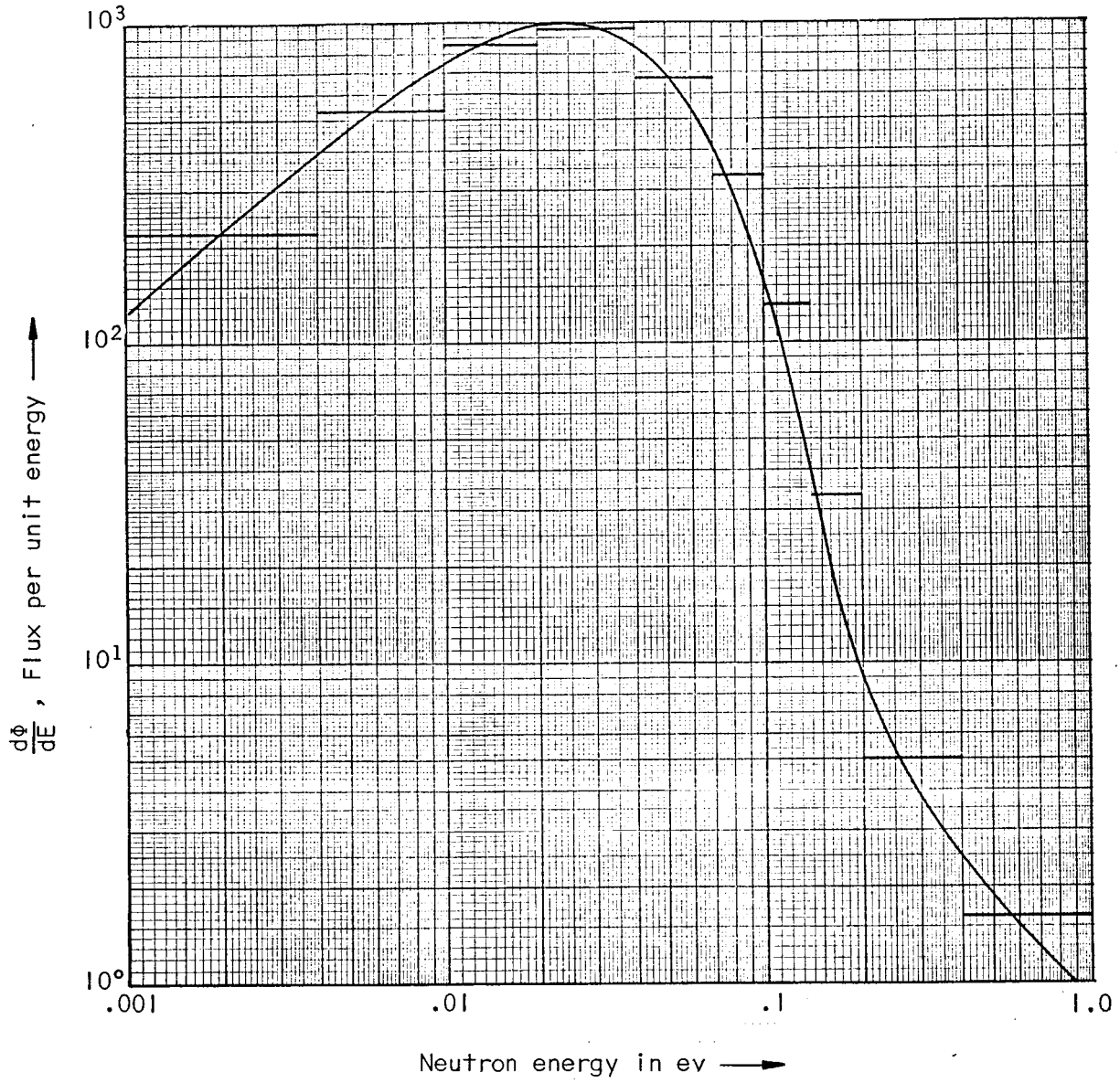

Figure 16.-- The solid curve is the experimental spectrum measured by Poole[18]. The histogram gives the calculated S_n flux spectrum at a radius of 44 cm in the single sphere system with no BF_3 filling.

T_a^i, the average neutron temperature for each group was obtained by a numerical integration of the formula

$$T_a^i = \frac{\int_{E_i}^{E_{Hi}} F(E)\, E/k\, dE}{\int_{E_{Li}}^{E_{Hi}} F(E)\, dE} \qquad (11)$$

where $F(E)$ is the thermal flux spectrum from the experimental work of Poole, and k is Boltzmann's constant. The values used for T_a^i are listed in Table 3.

TABLE 3

GROUP NEUTRON TEMPERATURES

WEIGHTED BY POOLE'S SPECTRUM

Group No. i	T_a^i, Group Averaged Neutron Temperature °K
19	1883.5
20	1336.0
21	958.4
22	616.0
23	344.4
24	176.7
25	84.6
26	31.8

If a neutron energy spectrum is Maxwellian, the energy distribution is given by the relation

$$n(E) = \left(\frac{E}{kT_e}\right)^2 \exp\left(-E/kT_e\right) \quad , \qquad (12)$$

where T_e is the effective neutron temperature. The average temperature of all neutrons in the Maxwellian spectrum is given by

$$\bar{T} = \frac{\int_o^\infty n(E)\ E/k\ dE}{\int_o^\infty n(E)dE} = 2\ T_e \quad . \qquad (13)$$

Thus, it is expected that the quantity labelled T_a on the figures is about twice the effective neutron temperature. This is only an approximation because although the fluxes calculated in the water by the S_n method seem to differ only slightly from Poole's spectrum and thus from the Maxwellian, the fluxes inside the cavity show a spectrum quite different from the Maxwellian. Also, unlike the flux, the average temperature is very sensitive to the choice of thermal energy cutoff.

Figure 17 shows the way the spectrum changes with increasing BF_3 pressure in the single sphere system. The histograms show the average cavity spectra from the S_n computations with 0.0, 0.5, and 1.0 atmosphere BF_3 filling. The upper line is nearly identical to Poole's spectrum, as in Figure 16. As might be expected, when there is no absorbing gas in the cavity, the spectrum inside the cavity is nearly identical to that in the water. The lines drawn through the histograms are not fitted curves, but are intended to make the histograms

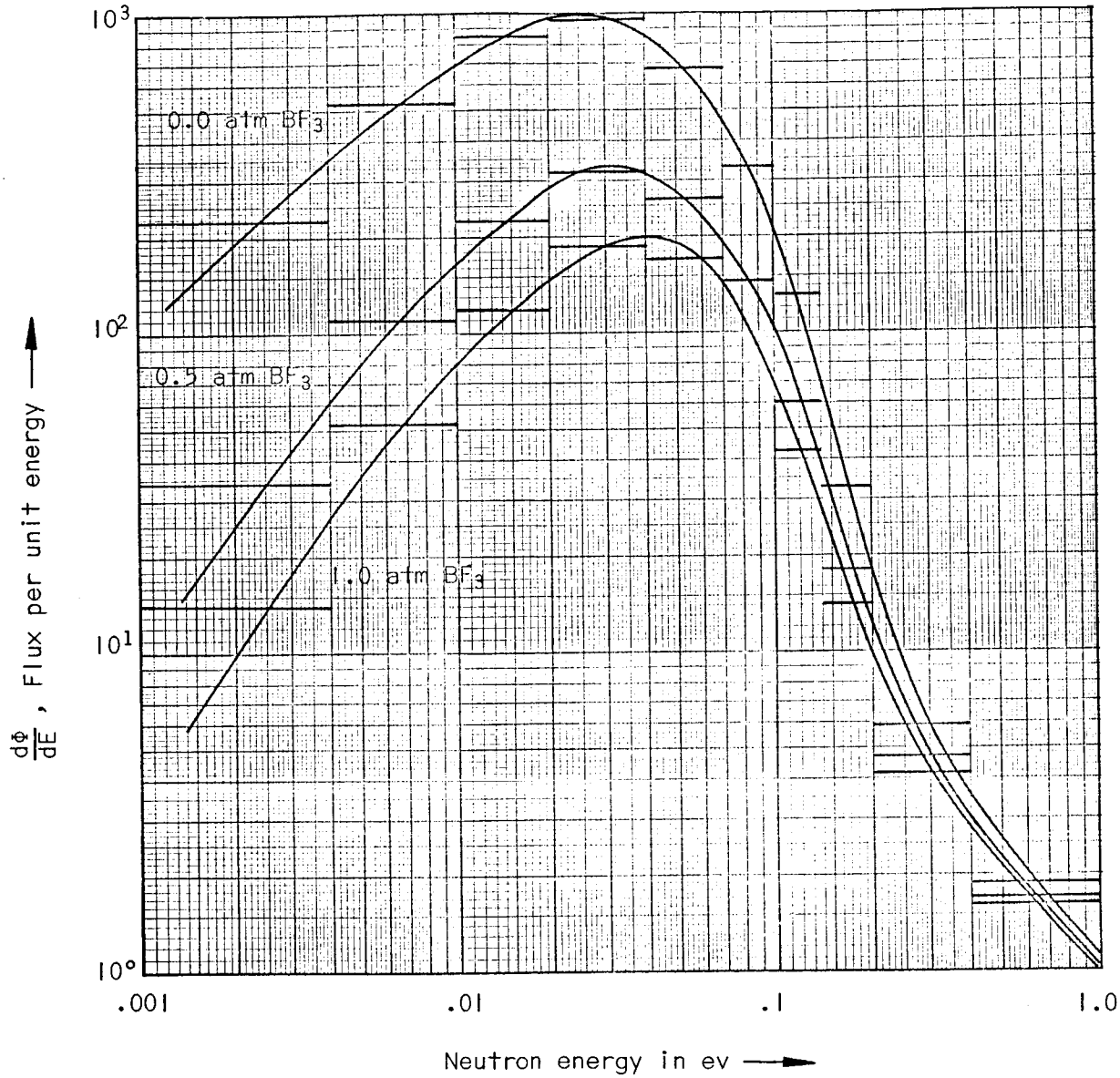

Figure 17. -- Average thermal neutron spectra in the cavity of the single sphere system with 0.0, 0.5, and 1.0 atmosphere of BF_3.

easier to read. It can be seen that the change in spectrum is most pronounced in the lower energy groups, for which the boron absorption cross section is much greater.

It is often stated that the Maxwellian spectrum will continue to have the Maxwellian shape with a higher effective temperature when a 1/v absorber is introduced into the system[19]. This, of course, is not true in a cavity system where the moderation is external to the absorber.

The average temperatures are one way of illustrating the fact that the thermal neutron spectrum changes from point to point within a given system. Figure 18 shows some typical spectrum histograms for three different locations in the nine-inch internal sphere system with 4 atmospheres BF_3 filling. Again it can be seen that the thermal flux spectrum in the BF_3 gas is quite different from that in the moderator, especially for the lower energies.

The benefits of a cross section set with many thermal groups and with upscattering are very great for a problem of this nature. As an example, consider the effective magnitude of the thermal absorption cross section of boron in the BF_3 gas when it is averaged over a calculated spectrum using the averaging procedure

$$\sigma_a^{Boron} = \frac{\sum_{i=19}^{26} \Phi_i \sigma_{ai}^B}{\sum_{i=19}^{26} \Phi_i} \qquad (14)$$

where Φ_i is the flux calculated by the S_n computation, and the σ_{ai}^B are the group absorption cross sections of boron from the library.

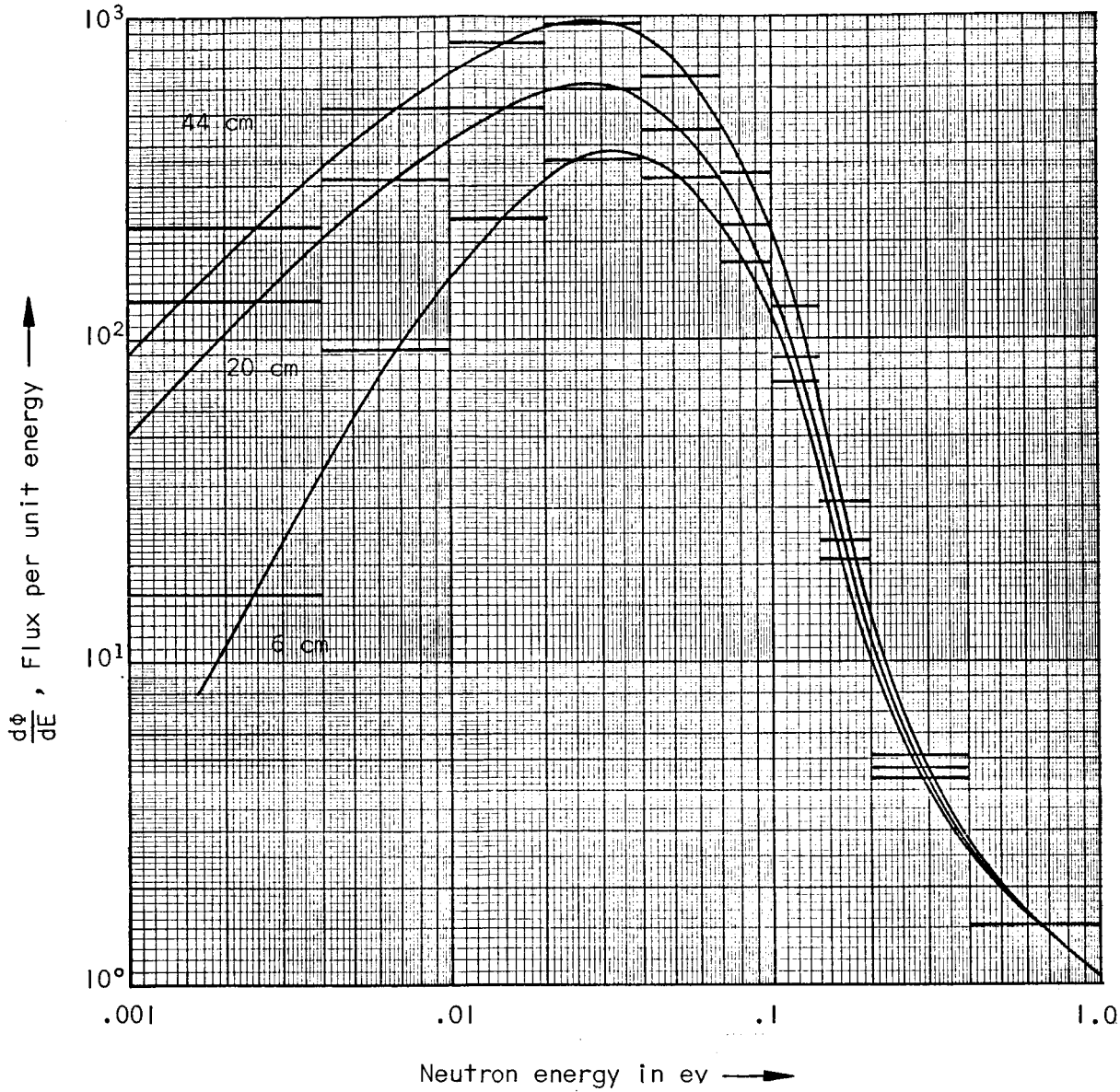

Figure 18. -- Thermal neutron spectra at radial distances of 6, 20, and 44 centimeters in the 9-inch internal sphere system with 4.0 atmospheres of BF_3 filling.

If Φ_i is the flux in the water or the flux in the cavity with no BF_3 filling, the average absorption cross section is 654 barns, which is fairly close to the Maxwellian average of 669 barns. The average value of this cross section decreases considerably as the BF_3 filling increases. With 0.5 atmosphere of BF_3 in the single sphere system, the spectrum average of this cross section varies in the gas from 585 barns at a distance of 3 centimeters from the center to 600 barns at 33 centimeters. Finally, if the averaging is done with the fluxes in the single sphere system with 1.0 atmosphere of BF_3, the average value of the absorption cross section of boron ranges from 550 barns at 3 centimeters to 580 barns at 33 centimeters.

These spectrum-averaged cross sections are only approximate, since the group cross sections in each case are all based upon the same spectrum; however, the group structure is sufficiently narrow that the change in spectrum within a group will result in a small change in the group cross section. The above calculations illustrate that the absorption cross section of boron varies by as much as 5 percent within the gas region itself, and varies by 16 percent from the gas to the moderator. From this it could be concluded that a calculation using only one thermal group would be inaccurate in predicting thermal absorption in an externally moderated system unless the thermal neutron spectrum in the absorber were known in advance and used to generate the cross sections.

It is here where other workers in the field of externally moderated reactors have been in greatest error. Using a single thermal energy group for a range of absorber concentrations is incorrect.

Specifically, taking the average absorber cross section to be the Maxwellian average at the moderator temperature will always give too low a critical mass; the magnitude of the error becomes greater as the concentration and energy dependence of the absorber cross sections increases.

REDUCTION OF S_n DATA TO FOIL ACTIVATIONS

The most common and the simplest way of comparing indium foil activation data to theoretical calculations is to reduce the foil data to thermal fluxes using formulae, graphs, or tables for the particular foil size which are available in the literature[20,21,22,23]. This method was used to find the experimental thermal fluxes shown on all of the figures in this and in the previous work reported. However, from the discussion on spectra, it is obvious that more information is available from the multigroup S_n calculations than was used in the determination of the theoretical thermal flux. It is known that the spectrum varies significantly in the system, and that the factors relating foil activation to thermal flux are spectrum dependent. A better comparison might therefore be made by reducing the S_n calculations to theoretical foil activations. It is quite difficult to take the spectrum into account when foil data are reduced to fluxes; it is somewhat less difficult to reduce the theoretical fluxes in a calculation with many thermal groups to theoretical foil activations.

First a correction is made for self shielding of neutrons in the foil. According to Hanna[21], this is the only effect for which correction is necessary if the foil is irradiated in a cavity so large that a vanishingly small number of neutrons passing through the foil are ever scattered back through the foil again. The correction for this effect has the form

$$\frac{A_c}{A_o} = \frac{(1/2 - E_3(\tau))}{\tau} (1 + \varepsilon) \qquad (15)$$

where τ is the foil thickness in mean free paths, $E_3(\tau)$ is the third order exponential function, and ε is a small edge correction factor.

In a scattering medium such as water, a correction is also made for the depression of the incident flux due to the absorption of the foil. Several formulae are reported for correcting for this effect, and all have the general form

$$F(\gamma,\tau) = \left[1 + [1/2 - E_3(\tau)]\, g(R,\gamma)\right]^{-1} \qquad (16)$$

where γ is defined as Σ_s/Σ_{total} for the scattering medium, R is the radius of the foil, and $g(R,\gamma)$ is a factor approximated by different methods by various authors. The Ritchie-Eldridge[22] method with an edge correction modification was chosen here since it was reported to give good agreement with the experiments done in water by Walker et al[20] with 2 cm diameter indium foils, and also by Shook et al[23] for dysprosium-aluminum foils.

In the Ritchie-Eldridge method, $g(R,\gamma)$ is evaluated from the formula

$$g(R,\gamma) = 3L/2\lambda \;\; S(2R/L) - K(2R/\lambda,\gamma) \qquad (17)$$

where L and λ are the diffusion length and total mean free path of water, respectively, and the function $S(X)$ is defined by the integral

$$S(X) = 1 - 4/\pi \int_0^1 \sqrt{1 - t^2} \;\; e^{-Xt}\, dt, \qquad (18)$$

$k(\chi,\gamma)$ is defined by

$$K(\chi,\gamma) = 1/2 \int_0^1 \frac{dy}{y} S\left(\frac{\chi}{y}\right) \frac{h(y,\gamma)}{1+h(y,\gamma)} , \qquad (19)$$

and the function $h(y,\gamma)$ is defined by

$$h(y,\gamma) = y\gamma \left\{ \ln \frac{1-y}{1+y} + \frac{y\gamma}{4} \left[\ln^2 \left(\frac{1-y}{1+y} \right) + \pi^2 \right] \right\} . \qquad (20)$$

To get the factors needed to reduce the multigroup data to foil activations, group self-shielded cross sections were computed by evaluating the integral

$$\sigma_i \begin{matrix} \text{self-shielded} \\ \text{activation} \end{matrix} = \frac{\int_{E_{Li}}^{E_{Hi}} F(E)\, \sigma_a(E)\, \frac{(1/2 - E_3(\tau(E)))}{\tau(E)} (1+\varepsilon) dE}{\int_{E_{Li}}^{E_{Hi}} F(E) dE} \qquad (21)$$

where $\sigma_a(E)$ is the absorption cross section of indium at energy E calculated from the resonance data published in reference 24, and $F(E)$ is Poole's spectrum. The integration was done by a 60-point strip integration procedure using a 6-point Newton-Cotes formula of closed type[25]. The $E_3(\chi)$ functions were calculated by evaluation of the series

$$E_1(\chi) = \sum_{n=1}^{\infty} \frac{\chi^n}{n \cdot n!} - .572216 - \ln\chi, \qquad (22)$$

combined with the recursion relation

$$E_n(\chi) = (e^{-\chi} - \chi E_{n-1}(\chi))/(n-1) \qquad (23)$$

The activation cross sections corrected for flux depression in the water were found by evaluation of the integral

$$\sigma \begin{matrix} \text{flux depression} \\ \text{activation}_i \end{matrix} = \frac{\int_{E_{Li}}^{E_{Hi}} \sigma_a(E) F(E) \left(\frac{1/2 - E_3(\tau(E))}{\tau(E)}\right)(1+\varepsilon)(1+ (1/2 - E_3(\tau(E))) g(R,\gamma)) dE}{\int_{E_{Li}}^{E_{Hi}} F(E)\, dE} \qquad (24)$$

where $g(R,\gamma)$ is defined in equation 23 and γ, L, and λ were calculated as a function of energy from cross section data taken from BNL 325[24,26]. For arguments less than 4, the function $S(\chi)$ was calculated by evaluating the series

$$S(\chi) = \frac{2}{\pi} \sum_{m=1}^{\infty} \frac{(-1)^{m+1} \chi^m \Gamma(\frac{m+3}{2})}{(m+1)! \Gamma(\frac{m+4}{2})} \qquad (25)$$

which is given as equation (33) in the report by Ritchie and Eldridge[22]. For arguments greater than 4, so many terms of the summation were needed that it was quicker to evaluate $S(\chi)$ by an 18-point strip integration of equation 24. The function $K(\chi,\gamma)$ was also calculated by the 18-point strip integration procedure. The functions $S(\chi)$ and $K(X,Y)$ calculated in this way reproduced the graphs of these functions given by Ritchie and Eldridge in reference 22. No significant difference was found between the edge effect correction used by Walker et al, who used

$$\varepsilon = \frac{\tau}{1/2 - E_3(\tau)} \times \frac{t}{R} \times (\frac{1}{\pi} - \frac{\tau}{6}) \qquad (26)$$

and that used by Shook et al, who did not use the ε factor, but instead calculated τ by the relation

$$\tau = (\frac{\Sigma_a + t}{1 + \frac{t}{R}}) \qquad (27)$$

where R is the foil radius, and t is the foil thickness.

Corrected group absorption cross sections for the indium foils used in the experiment were calculated by numerical integration of equations (21) and (24). These data and the corresponding uncorrected

group cross sections are listed in Table 4. The correction group absorption cross sections were used to calculate theoretical foil activation from the multigroup S_n fluxes using the summation

$$\text{Activation}(r) = \frac{\sum_{i=13}^{26} \sigma_{\text{abs } i}^{\text{corrected}} \Phi_i(r)}{\sum_{i=13}} \qquad (28)$$

where in the cavity $\sigma_{\text{abs } i}^{\text{corrected}}$ is the indium group absorption cross section corrected only for self-shielding, and in the water it is the group absorption cross section corrected for both self-shielding and flux depression.

Some errors are evident in the calculation of the corrected cross sections, but it is expected that they are minor. First, the correction equations assume an isotropic flux. The error introduced because of this is probably small because the gradient is small compared to the mean free path of the neutrons in water everywhere except at the interface. Some error may also come into the group cross sections because they are weighted by a water spectrum instead of the actual spectra. However, since narrow energy groups are used, this should be small. As a check upon this effect, an identical set of calculations was performed with unit weighting; the corrected group absorption cross sections calculated in this way differed at most by three percent from those weighted by Poole's spectrum.

Figure 19 is an example of the theoretical indium activation calculated from the S_n fluxes using equation (28) and the data in Table 4. No flux depression correction was made anywhere in the cavity, and the flux depression was assumed to be constant for all points in

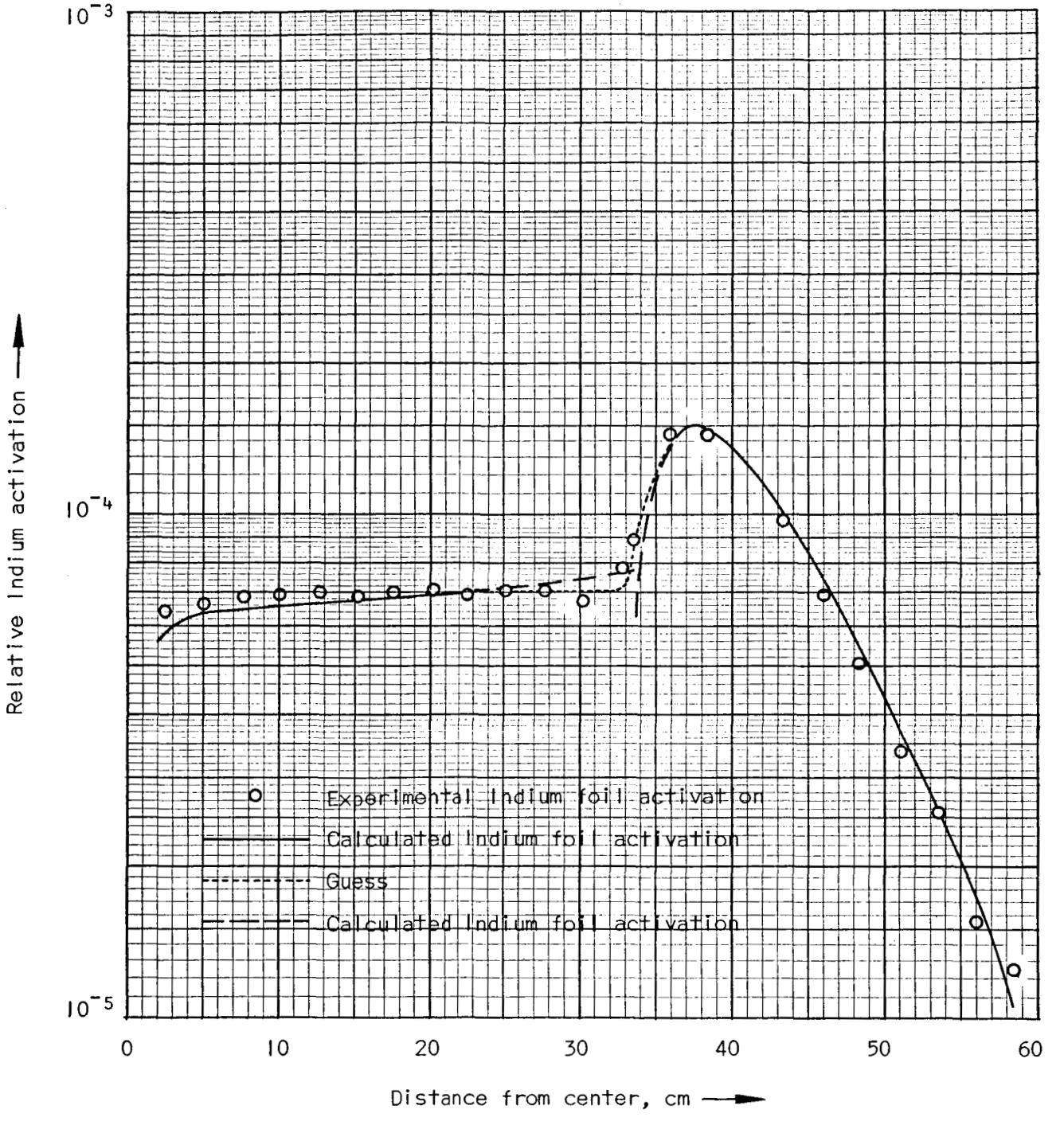

Figure 19. -- Comparison of experimental and calculated indium foil activation for the single sphere system with 1.0 atmosphere BF_3 filling.

TABLE 4

GROUP ABSORPTION CROSS SECTIONS FOR 1.2-cm-diameter, .005-inch-thick INDIUM FOILS IN WATER: UNCORRECTED, CORRECTED FOR SELF-SHIELDING, AND CORRECTED FOR BOTH SELF-SHIELDING AND FLUX DEPRESSION

Group Number i	E_{Li} - E_{Hi} Energy Range, ev	Average σi Barns	Self-Shielded Flux σi Barns	Depression σi Barns
13	30 - 100	1.4	1.3	1.3
14	10 - 30	24.3	15.1	9.3
15	3 - 10	60.6	44.1	33.3
16	1 - 3	2504.9	381.1	218.3
17	.4 - 1	137.3	119.3	103.9
18	.2 - .4	87.5	80.0	72.7
19	.14 - .2	94.2	85.6	76.7
20	.1 - .14	104.2	93.9	82.8
21	.07 - .1	117.4	104.7	90.5
22	.04 - .07	141.2	123.6	103.0
23	.02 - .04	183.6	156.0	121.2
24	.01 - .02	251.4	204.2	143.2
25	.004 - .01	362.5	275.3	170.7
26	.001 - .004	599.4	400.7	209.4

the water. This is not correct near the interface either in the water or in the cavity. For cavity foils located within a few foil diameters of the interface, some flux depression would exist, and so the activation there would actually be less than that given by equation (28).

For in-water foils located so near the interface that some of the neutrons passing through them could also have passed through the cavity, the flux depression correction is too great, and thus the actual activation would be less than is given by equation (28). It is reasonable to expect the foil activation to be continuous across the interface, while the use of a constant correction for all points in a region causes the calculated activations to be discontinuous. Thus, near the interface in Figure 19, dashes are used to show the calculated activation, while the dotted lines show a guess of what the foil activation might be if the correct flux depression factors could be found for these points.

The calculated activation does not include neutrons above 100 ev in energy, and so a correction was made to the first five experimental data points to subtract the small amount of 54-minute activity which is caused by fast neutrons from the source. The amount of the correction was determined experimentally by counting cadmium-covered foils which had been irradiated at various distances from the unmoderated source.

The experimental activations agree with the calculated activation. However, it cannot be stated definitely that the agreement between experiment and theory is better than in Figure 4, where experimental flux is compared to theoretical flux for the same system. The difference between these two comparison methods is smaller than the experimental uncertainties, especially the asymmetry of the source emission and the perturbing effect of the through-tube.

CAUSES OF THE PEAKING PHENOMENON

Two possible causes of the peaking phenomenon have been mentioned in previous sections. These will be summarized here, and a third equally probable cause will be cited.

First it must be mentioned that the experimental work is divided chronologically into two periods. The work done in the first period is described in reference 1. The more recent work used the same four-pi gas flow counter and the same irradiation procedure, but the counting procedure and data reduction methods were quite different. The latter have been described above. None of the experimental fluxes in the second period show peaking at the center of the sphere, although some of the sphere systems measured were identical to those which showed peaking in the first period.

One suspected cause of peaking is the asymmetry of the Pu-Be source. Such asymmetry probably would cause the activations measured in the through-tube to be greater in the center and less at the interface than would be measured with a symmetric source. However, it is unlikely that this was the only or the major cause, since the same source was used in both periods.

The S_n and age-integral transport solutions show that highly absorbing deposits at the interface do cause peaking toward the center. There may have been deposits of boron on the inside of the sphere; early in the first experimental period a leak developed in the single sphere system with one atmosphere of BF_3 filling. When the leak

was discovered the sphere was nearly half full of water and all of the gas had reacted with the water. It is likely that some of the reaction products of BF_3 and water form insoluble compounds with aluminum. The measurements were continued after the leak had been repaired and the inside of the sphere had been washed with deionized water and air dried. A new single sphere system was made with new aluminum hemispheres for the more recent experimental work and this could explain why no peaking is observed in the thermal fluxes measured in the second period. On the other hand, the shape of the peaking calculated by the two theoretical methods is quite different than that which was observed experimentally (compare Figures 14 and 15 to Figure 20).

The third possibility, which has not been mentioned until now, is that some errors may have been involved in the correction of the activation data for the 4-1/2 hour activity of indium-115. As was reported in reference 1, the amount of this activity was found by taking repeated counts of a few foils which had been irradiated with cadmium covers, so that the shape of the decay curve could be found. The relative fractions of 4-1/2 hour and 54-minute activity for cadmium-covered foils could then be found. The assumption was made that the amount of 4-1/2 hour activity which was produced was dependent only upon irradiation position and irradiation time, and not upon BF_3 pressure or whether the foil was covered with cadmium during irradiation. It is possible that the correction factors used were not sufficient, or were not applied properly to the experimental data.

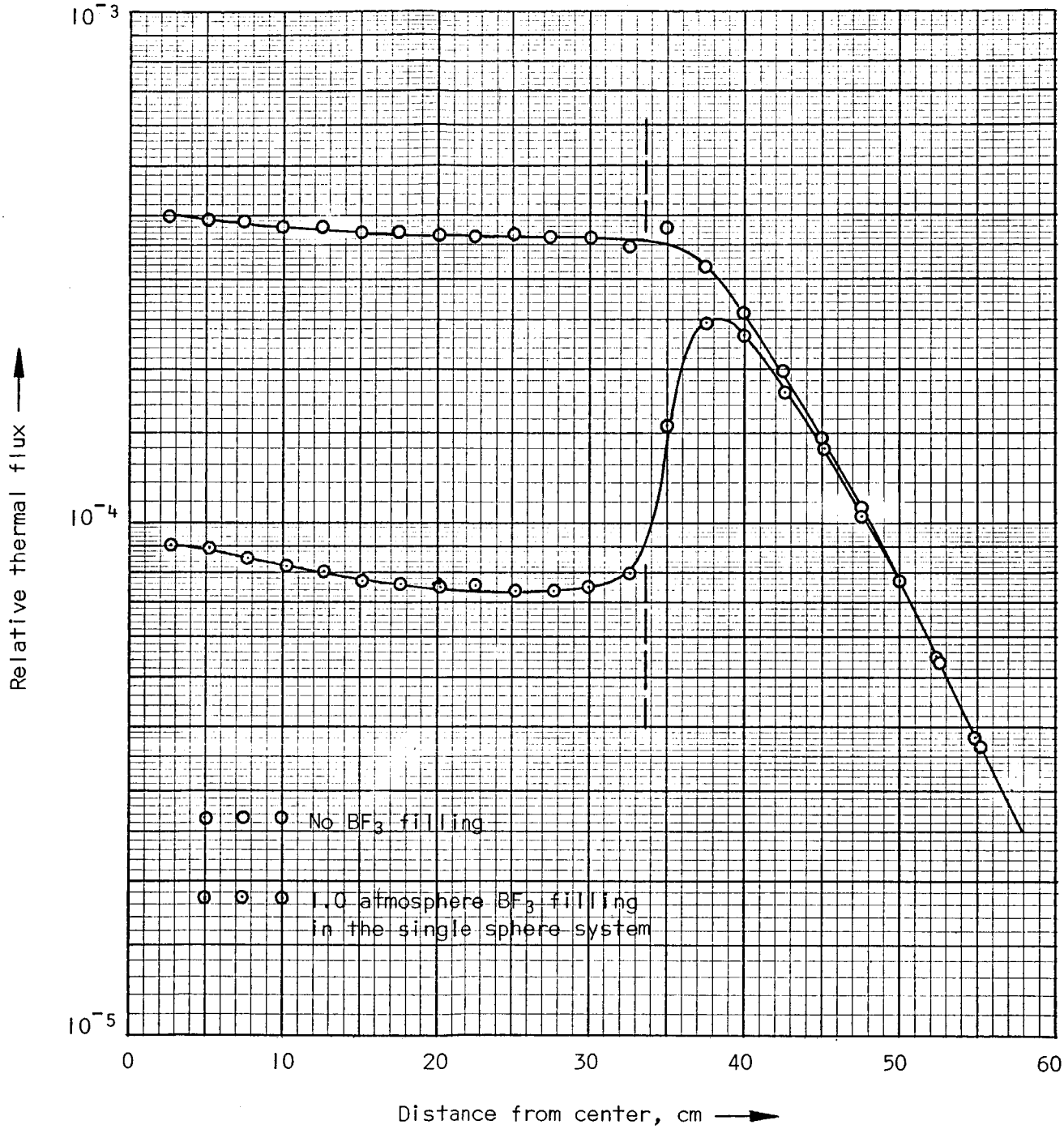

Figure 20. -- Experimental thermal fluxes from reference 6 showing the 'peaking' effect in the center of the cavity.

Since the fast neutrons which cause the 4-1/2 hour activity come from the source, it would be expected that the amount of this activity would fall off as $1/r^2$ at distances from the source large enough that the source looks like a point source. This possibility seems likely, since the difference between the experimental data and a flat flux in the cavity goes roughly as $1/r^2$. The data reduction method in the second period used a more reliable method for correction for this activity, and thus such peaking, if it is due to 4-1/2 hour halflife activity, would not be found in those data.

In summary, this work has found three possible causes for the peaking phenomenon reported in reference 1. It has not been possible to pinpoint any single cause. However, it has been established by theoretical calculations and further experiments that the peaking reported in reference 1 is not the correct flux shape in a water-BF_3 system with the gas uniformly distributed in the cavity and with a uniformly emitting source of fast neutrons at the center.

CONCLUSIONS

1. Thermal flux distributions calculated by three theoretical methods were found to agree with those measured by indium activation for single sphere systems. For systems with the absorbing gas confined to a smaller internal sphere, the theoretical fluxes agree with the experiments only in the moderator and void region, and not inside the internal sphere. It is suspected that the experimental data are in error in this region because of neutron streaming in the tube passing through the center of the internal sphere, in which the indium foils were located.
2. The flux shapes calculated by S_n theory and diffusion theory were found to be quite similar for single sphere systems and quite different for systems with internal spheres. The diffusion theory fluxes are greater in magnitude for all systems, and so diffusion theory calculations would be expected to give a lower critical mass than S_n calculations. It is concluded that the use of diffusion theory in a cavity system is questionable unless comparisons are first made with a more rigorous theory.
3. The use of age theory in the moderator coupled with an integral transport method for the cavity gives thermal flux distributions which are close to those found by S_n calculations, but with somewhat lower fluxes in the absorbing gas. It is believed that

this is due to the use of a single average thermal absorption cross section for the gas in the integral transport solution, which did not take into account the difference in thermal neutron spectrum between the cavity and moderator.

4. The multigroup S_n calculations indicate that there is a considerable change in thermal neutron spectrum inside the cavity and thus that using a multigroup cross section set with only one thermal group would be incorrect unless the spectrum were known in advance.

5. A comparison of theoretical indium foil activation with experimental foil activation was attempted. It was not possible to judge definitely whether this method of comparison is better than comparing experimental fluxes with theoretical fluxes because of experimental perturbations caused by the presence of the through-tube and asymmetry in the fast neutron emission of the Pu-Be source.

NOMENCLATURE

A	Atomic mass
D_x	Diffusion coefficient in region x
E	Neutron energy
E_{Li}	Low energy limit of energy group i
E_{Hi}	High energy limit of energy group i
f_i	Fraction of neutrons in the source spectrum which are in group i
$F(E)$	Neutron energy spectrum used as a weighting function in an integration
Φ	Neutron flux
$\Phi_p(r)$	Flux due to a point source of neutrons in a moderator with no cavity
$\Phi_v(r)$	Flux in the moderator due to a point source of neutrons at the center of a spherical void
γ	Interior greyness = $\frac{\text{net current into interior}}{\text{flux at interior boundary}}$
$I_{i\rightarrow j}$	Fraction of scatterings in energy group i which result in an energy change such that the resultant neutron energy is within the limits of energy group j
L	Thermal neutron diffusion length
$q(r)$	Magnitude of emission of a source of neutrons at r
R_o, a	Radius of outer sphere
R_i	Radius of inner sphere
R_s	Radius of source
S_i	Neutron source in energy group i
$\Sigma(E)$	Energy dependent macroscopic cross section
$\sigma(E)$	Energy dependent microscopic cross section
σ_i	Average cross section in energy group i

$\Sigma_{i\to j}$	Σ_s for group i times $l_{i\to j}$
$\sigma_{i\to j}$	σ_s for group i times $l_{i\to j}$
$T_{effective}$	Effective neutron temperature of a Maxwellian distribution
T_a^i	Average temperature of all neutrons in energy group i
T_a	Average temperature of all the neutrons in groups 19 through 26 in the energy group structure used here
$\tau(E)$	Age to the 1.457 ev indium resonance as a function of energy
τ^{in}	Average age to the indium resonance
upscattering	Scattering of neutrons which results in a net increase in neutron energy
v	Neutron velocity

Subscripts:

a	Absorption
i	Average for group i
r	Removal from energy group
s	Scattering
t	Total
tr	Transport

1. Floro D. Miraldi, David McBride and George W. Nelson, Experimental Neutron Flux Distributions in a Water System with an Internal Cavity. NASA report CR-54110 (June, 1964).

2. George W. Nelson, Thermal Neutron Flux Distributions in a Water System with an Internal Catity, Ph.D. Thesis, Case Institute of of Technology (November, 1966).

3. R. J. Howerton, J. Bengston, and S. J. French, Table of Two U^{235} Fission Spectra. USAEC report UCRL-5208 (October, 1957).

4. M. E. Anderson and W. H. Bond, Neutron Spectrum of a Plutonium-Beryllium Source. Monsanto Research Corporation report MLM-1131 (1963).

5. C. B. Mills and F. Brinkley, A One Dimensional Intermediate Reactor Computing Program. USAEC report LA-2161 (March, 1959).

6. Robert G. Ragsdale and Robert E. Hyland, Some Nuclear Calculations of U^{235}-D_2O Gaseous-core Cavity Reactors. NASA report TN D-475 (1961).

7. Robert E. Hyland, Robert G. Ragsdale, and Eugene J. Gunn, Two-dimensional Criticality Calculations of Gaseous-core Cylindrical-cavity Reactors. NASA report TN D-1575 (March, 1963).

8. T. F. Plunkett and R. J. Holl, Nuclear Analysis of Gaseous Core Reactors. Douglas Aircraft Company, Inc. report SM-44041 (May, 1963).

9. M. K. Butler, G. Duffy, H. Greenspan, E. Mueller, S. Sparck, and J. Zapatka, SNARG I-D. Argonne National Laboratory Applied Mathematics Division Technical Memorandum 95 (June, 1965).

10. Bengt G. Carlson, The S_n Method and the SNG Code. USAEC report LAMS-2201 (April, 1959).

11. Bengt G. Carlson, Numerical Formulation and Solution of Neutron Transport Problems. USAEC report LA-2996 (April, 1964).

12. R. T. Ackroyd and E. D. Pendlebury, "Survey of Theoretical Calculational Methods," pp. 47-118 of Criticality Control in Chemical and Metallurgical Plant. (Karlsruhe Symposium, 1961), Paris, O.E.C.D. European Nuclear Energy Agency.

13. Clarence E. Lee, The Discrete S_n Approximation to Transport Theory. USAEC report LA-2595 (March, 1962).

14. P. R. Wallace and J. LeCaine, Elementary Approximations in the Theory of Neutron Diffusion. Atomic Energy of Canada, Limited report AECL 336 (August, 1943).

15. R. R. Coveyou and J. G. Sullivan, "Calculations of Neutron Ages in Various Media," Neutron Physics Division Annual Report. USAEC report ORNL-2609, pp. 82-83 (February, 1958).

16. Reactor Physics Constants, USAEC Report ANL 5800, Second Edition (July, 1963). p. 133.

17. F. A. Valente and R. E. Sullivan, "The Age of Plutonium-Beryllium Neutrons in Light Water," Nuc. Sci. and Eng. 6, 162, 1962 (August, 1959).

18. M. J. Poole, "Measurement of Neutron Spectra in Moderators and Reactor Lattices. J. Nuclear Energy, 5, 325 (1957).

19. A. M. Weinberg and E. P. Wigner, The Physical Theory of Neutron Chain Reactors. Chicago: University of Chicago Press, 1958, pp. 342-343.

20. Jack V. Walker, John D. Randall, and Ronald C. Stinson, Jr., "Thermal Neutron Flux Perturbations Due to Indium Foils in Water," Nuc. Sci. and Eng. 15, 325-337 (1963).

21. G. C. Hanna, "The Thermal Neutron Flux Perturbation Due to an Absorbing Foil: A Comparison of Theories and Experiments," Nuc. Sci. and Eng. 15, 325-337 (1963).

22. R. H. Ritchie and H. B. Eldridge, "Thermal Neutron Flux Depression in Absorbing Foils," Nuc. Sci. and Eng. 8, 300-311 (1960).

23. Donald F. Shook, Donald Bogart, Donald L. Alger, and Robert A. Mueller, Thermal Neutron Flux Perturbation by Dysprosium-Aluminum Foils in Water and Uranyl Fluoride-Water Solutions. NASA report TN D-3237 (March, 1966).

24. D. J. Hughes and R. B. Schwartz, Neutron Cross Sections. USAEC report BNL-325, Second Edition (July, 1960).

25. F. B. Hildebrand, Introduction to Numerical Analysis. New York: McGraw-Hill Book Company, 1956, p. 73.

26. John R. Stehn, Murrey D. Goldberg, Benjamin A. Magurno, and Renate Wiener-Chasman, Neutron Cross Sections. USAEC report BNL-325, Second Edition, Supplement No. 2, (May, 1964).

27. R. D. Doctor and M. A. Boling, A 23-Group Neutron Thermalization Cross Section Library. Atomics International report NAA-SR-MEMO 8742 (July, 1963).

28. G. E. Hansen and W. H. Roach, Six and Sixteen Group Cross Section Sets for Fast and Intermediate Critical Assemblies. USAEC report LAMS-2543 (November, 1961).

Appendix A

Neutron Lifetime Measurements

The mean neutron lifetime of two systems were measured using a pulse-neutron technique. A complete study was not undertaken and only a few measurements were made to determine an approximate lifetime value for these systems. The systems examined were the single sphere with 0.5 atmosphere of BF_3 and the nine inch inner sphere system with an air filling.

The neutron source was a pulsed deuteron beam on a trituim target using a 400 KEV Van de Graaff accelerator as the deuteron beam generator. The accelerator beam tube was moved through a porthole in the water tank and brought to the sphere surface. The ideal position of the target would have been the center of the sphere system but this was not possible. Furthermore, the decay of the system is considered to be independent of the position of the pulsed source once the higher harmonics are gone.

Both BF_3 proportioned counters and a neutron scintillation crystal were used as detectors. The scintillation crystal system was preferred because it had a higher count rate, but because of its bulky geometry, it could only be used in the water and not inside the cavity. The results obtained with either detector at the same position agreed well. The detector signals were fed into a TMC model CN 110, 256 channel analyzer with a time analyzer plug-in unit along with the triggering pulses from the neutron generator. The channel width used was 50 microseconds.

Figure A-1 gives the major results of the measurements with the simple sphere with 0.5 atmosphere of BF_3. A value of 343 microseconds was obtained at the sphere center using a BF_3 counter in the through-tube. This value did not change significantly until the cavity-water interface was reached. The lifetime was very sensitive to position in this region and dropped rapidly as the position was moved into the water up to a distance of about two to three inches from the sphere surface. The lifetime value then stabilized to about 222 microseconds for the next few inches. The value in the water shown in Figure A-1 was taken at a distance of about four inches from the sphere surface. As a comparison, the calculated lifetime for an infinite system of water is 206 microseconds and for an infinite system of BF_3 at 0.5 atmosphere pressure is 452 microseconds.

The air filled, nine inch, inner sphere system gave results presented in Figure A-2. Data were taken at four different positions: at the center, at the inner interface, at the outer interface, and in water. Only one curve is shown for the internal measurements since they were all approximately the same. As expected the lifetime inside the sphere was very long: 881 microseconds at the center and 924 microseconds at the inner interface. The lifetime dropped off sharply at the water boundary to give a value of 252 microseconds at a distance of four inches from the sphere surface. The in-water curve showed a significant deviation from the expected exponential decay starting about 450 microseconds after pulse cutoff. One possible interpretation of the slower decay is that the cavity is acting as a net source of neutrons and the decay curve shows what might be termed "inner sphere return."

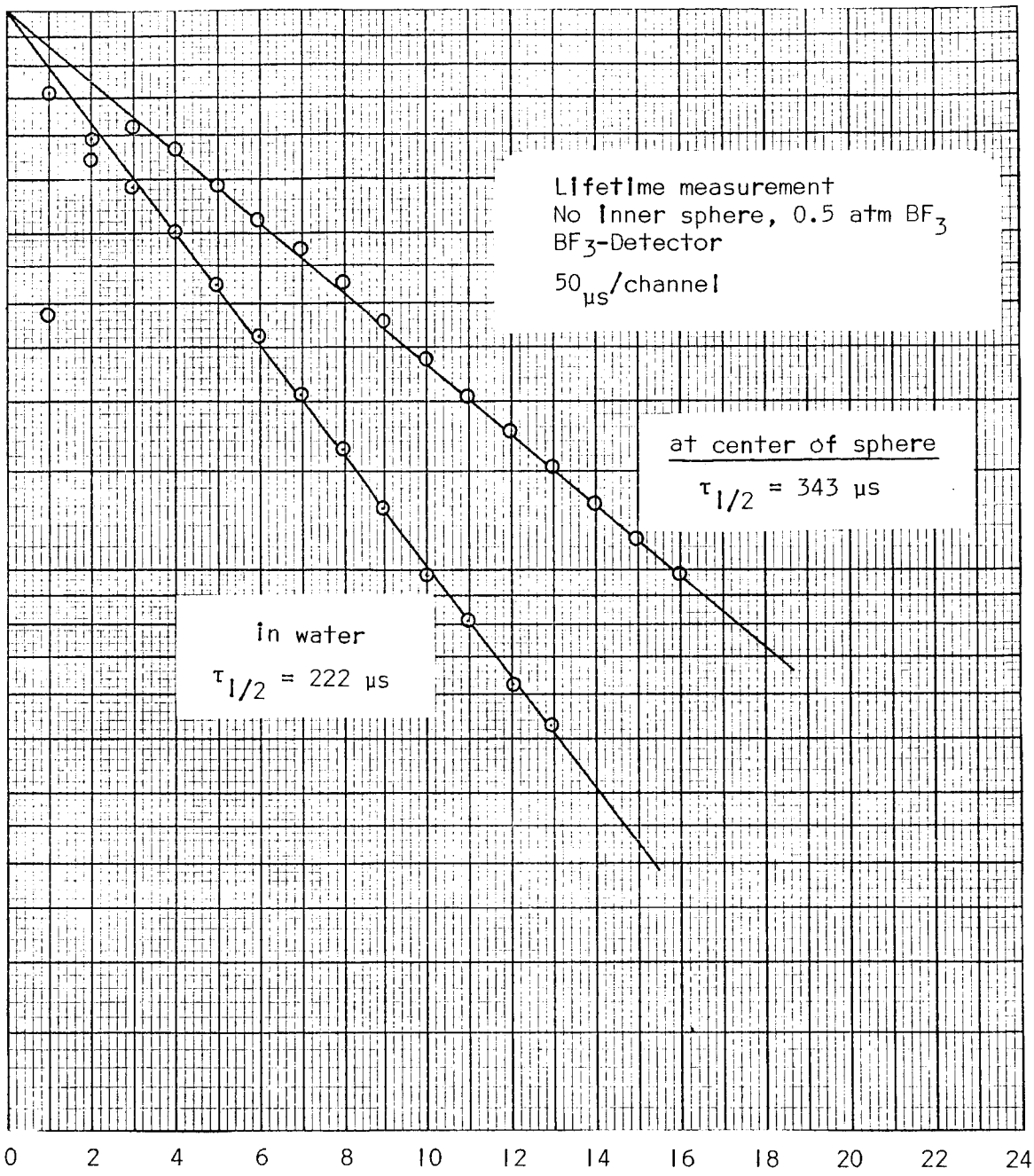
Lifetime measurement
No inner sphere, 0.5 atm BF_3
BF_3-Detector
50 µs/channel
at center of sphere
$\tau_{1/2}$ = 343 µs
in water
$\tau_{1/2}$ = 222 µs
Relative count rate/channel
0
2
4
6
8
10
12
14
16
18
20
22
24
Channel number

Figure A-1

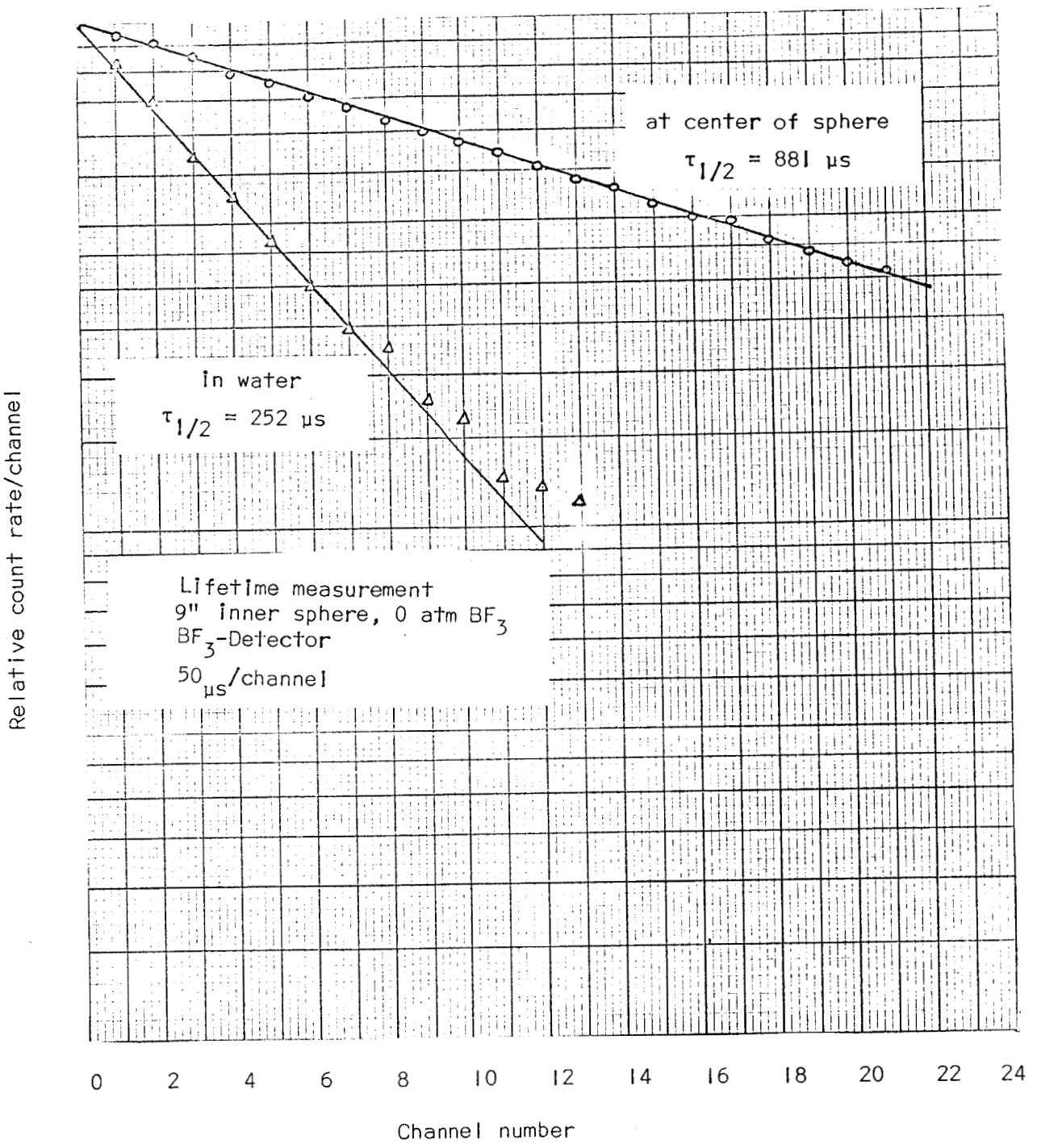
at center of sphere
$\tau_{1/2}$ = 881 μs
in water
$\tau_{1/2}$ = 252 μs
Lifetime measurement
9" inner sphere, 0 atm BF_3
BF_3-Detector
50 μs/channel
Relative count rate/channel
0
2
4
6
8
10
12
14
16
18
20
22
24
Channel number

Figure A-2

Appendix B

SELECTION OF GROUP CROSS SECTIONS

After the selection of a method of attack, the first problem in any nuclear reactor calculation is the selection of the cross sections and other nuclear data which are used by the method. For S_n and diffusion theory calculations, these data are the multigroup cross sections and their associated scattering matrices. For age calculations, the age from the source energy to thermal is needed, as well as the cross section data to describe the thermal neutrons.

In the S_n and multigroup diffusion calculations done here, two requirements existed which called for a multigroup cross section set different from those which are most often used for reactor calculations. Most cross section sets available in the literature are based upon a fission neutron spectrum, which is very different from the plutonium-beryllium source spectrum (see Figure I for a comparison of these spectra). In addition to the weighting of the cross sections in the higher energy groups by the fission spectrum, these sets have the added disadvantage of having too coarse a group structure in the Mev range to describe the Pu-Be spectrum. Most such sets have only one group over which to average the cross sections of all neutrons above 3 Mev in energy. As can be seen in Figure I, this would be sufficient for a fission spectrum since only a small fraction of fission neutrons have this high energy. Most of the neutrons in the plutonium-beryllium spectrum are above 3 Mev in energy, however, and a considerable fraction are in the 6 to 10 Mev range.

The second requirement is that the multigroup cross section set to be used must give a good description of neutron thermalization. This means that the thermal energy range should be divided up into several groups, with up-and down-scattering between these groups. This is necessary because a considerable change in neutron spectrum can be expected between the water and the highly absorbing BF_3 gas in the cavity. Furthermore, the absorption cross section of boron varies by nearly a factor of ten from the lower to the upper energies of the thermal spectrum, so a one-thermal-group, average value for this cross section is not justified. In addition to permitting a more accurate calculation of thermal neutron flux, the group fluxes generated with a cross section set having many groups in the thermal range would give a good idea of the neutron spectrum itself.

The set used in the calculations was based on A 23-Group Neutron Thermalization Cross Section Library, by R. D. Doctor and M. A. Boling of Atomics International[27]. This library is an extension of the Hansen-Roach set for fast and intermediate reactors[28]; it was extended to include neutron thermalization by the addition of nine groups which contained both up- and down-scattering, and which covered the energy range from .001 to .2 ev.

The group structure in the Mev range was too coarse to describe the Pu-Be source spectrum. This was corrected by reconstructing the group structure at the high energy end, as follows:

Old Set		New Set	
Group No.	Energy	Group No.	Energy
1	3.0 - ∞ Mev	1	8.0 - 10.5 Mev
2	1.4 - 3.0	2	6.5 - 8.0
3	0.9 - 1.4	3	4.0 - 6.5
		4	2.5 - 4.0
		5	1.4 - 2.5
		6	0.9 - 1.4

(Groups 6-26 of the new set are identical to 3-23 of the old set).

In order to find cross section values for these new groups, cross section data were taken from BNL-325, UCRL-5351, and UCRL-5226. These data were group averaged into the new group structure by the numerical evaluation of the integral

$$\sigma_i = \frac{\int_{E_{Li}}^{E_{Hi}} \sigma(E)\ F(E)dE}{\int_{E_{Li}}^{E_{Hi}} F(E)dE} \qquad (B1)$$

where E_{Hi} and E_{Li} are the upper and lower energy limits of group i, $\sigma(E)$ is the energy-dependent cross section data, and $F(E)$, the neutron energy spectrum, is taken as $1/E$*. The new elements of the scattering matrix, giving the fraction of neutrons scattered from

*For neutrons from a monoenergetic source slowing down in a weakly absorbing moderator, the asymptotic energy spectrum goes as 1/E. This spectrum is approached closely after a few collisions in oxygen, and is reached after the first collision in hydrogen. Since the Pu-Be source is not monoenergetic, this is only an approximation and is justified only because the energy groups are narrow. A better choice for F(E) might be found either by Monte Carlo or iterative multigroup calculations.

group to group were calculated by evaluating the integral

$$l_{i\to i+1} = \frac{\int_{E_{Li}}^{\text{Min}\,(E_{Hi},E_{Li}/\alpha)} \frac{E_{Li} - \alpha E_o}{(1-\alpha)E_o}\,\frac{1}{E_o}\,dE_o}{\int_{E_{Li}}^{E_{Hi}} \frac{1}{E_o}\,dE_o} \qquad (B2)$$

where $\alpha = (\frac{A-1}{A+1})^2$, and $l_{i\to i+1}$ is the fraction of neutrons scattered from the ith to the i plus first group. This was sufficient for all materials except hydrogen, for which scattering to all lower energy groups is possible. For hydrogen the other scattering matrix elements were calculated from the relation

$$l_{i\to i+k} = l_{i\to i+1}\,\frac{E_{Hi+k} - E_{Li+k}}{E_{Li}} \qquad (B3)$$

The 23-group library of Doctor and Boling contains all of the isotopes needed for the calculation except fluorine, tantalum, maganese and plutonium. Cross section data for groups 1 through 6 for these elements were generated in the same way as for those which were present, as described above. The same method was used to generate data for groups 7 through 17 for manganese and tantalum, while data for fluorine and plutonium in these groups was available from the original Hansen-Roach set in reference[28].

Group total cross sections for the nine thermal groups were calculated by numerical integration of the formula

$$\sigma_{ti} = \frac{\int_{E_{Li}}^{E_{Hi}} F(E)\ \sigma(E)dE}{\int_{E_{Li}}^{E_{Hi}} F(E)dE} \qquad (B4)$$

where $\sigma(E)$ is tabular data from BNL-325 and its supplements and $F(E)$ is Poole's experimental thermal neutron spectrum for water (see Figure 16), which is the spectrum the authors of the 23-group library used to calculate their water cross section data . . This still gave only total cross sections. On the basis of thermal cross section data from ANL-5800, σ_a for maganese and fluorine was taken as $1/v$ and σ_s was calculated as $\sigma_t - \sigma_a$. For plutonium and tantalum σ_s was assumed constant and σ_a was calculated as $\sigma_t - \sigma_s$.

Since energy transfer in the scattering of thermal neutrons by atoms is primarily dependent on atomic weight, thermal scattering matrices for these four missing elements were derived from those of elements which were present in the 23-group library. The thermal scattering matrix of plutonium was assumed to be the same as U^{235}, and that of manganese was assumed to be the same as iron (The atomic weight of Mn is 54.9, compared to 55.8 for Fe). The thermal scattering matrix of fluorine was based on oxygen and that of tantalum on U^{235} , but it was modified slightly to make up for the difference in atomic weight.

$l^{A}_{i\rightarrow i}$ is the diagonal, or self-scattering, element of the scattering matrix of isotope A, and thus is the probability that a neutron does not enter a different energy group upon scattering from an

atom of this isotope. The probability that the neutron does enter a different energy group is $(1-l^{A}_{i\rightarrow i})$. It was observed that for any two different isotopes A and B, the ratio $R_{AB} = \frac{(1 - l^{A}_{i\rightarrow i})}{(1 - l^{B}_{i\rightarrow i})}$ is practically constant over the group structure for groups 1-17. This ratio was also observed to be roughly constant for groups 18-26 for most of the elements in the library. Assuming the same ratio to hold for all groups, if B were an isotope for which the scattering matrix elements were known, and if those for A were unknown, then a rough correction could be made that $l^{A}_{i\rightarrow i\pm k}=R_{AB}l^{B}_{i\rightarrow i\pm k}$, except for the case when k = 0, for which $l^{A}_{i\rightarrow i}=1-R_{AB}(1-l^{B}_{i\rightarrow i})$. It was found from the other data in the library that there was an increase of 32 percent in off-diagonal scattering matrix elements going from uranium to tantalum, and a decrease of 18 percent going from oxygen to fluorine.

This is a rough correction at best, and its validity will decrease as the difference in atomic weight increases. Such a correction will not, of course, be valid at all when isotopes A and B are in different physical forms, as, for example, a metallic solid and a gas.

Although some arbitrariness exists in the cross sections of these four missing elements, their ultimate values should have little effect on the final flux distributions. For example, the element fluorine occurs only in the gas BF_3, in which both the absorption and scattering cross sections of fluorine are small compared with the absorption cross section of boron. The metals plutonium, maganese,

and tantalum are homogenized together with the iron, nickel, chromium, and beryllium into a small source metal sphere at the center of the cavity; this sphere of source metals is nearly "black" to thermal neutrons, so some small error in the cross sections of a few of the elements can be tolerated.

The plutonium in the source was considered to be non-fissionable, since the fast fission in the plutonium is already taken into account in the source spectrum[4], and the thermal neutron flux, which is much less than the fast flux, is attenuated by the outer shells of stainless steel and tantalum.

APPENDIX C

SOURCE EMISSION ASYMMETRY

AND ITS EFFECT UPON THE EXPERIMENTAL FLUX DISTRIBUTIONS

When the experimental project was first undertaken, it was assumed that the emission of fast neutrons from the plutonium-beryllium source, when observed at large distances, would be close to that of a point source. It was later found that this was not true, so that the experimental results may be somewhat in error. In this appendix, measurements of the magnitude of this source asymmetry are reported, and some conjectures are presented as to the effects this asymmetry might have on the experimental data.

As a check on the magnitude of the source asymmetry effect, the fast neutron flux was measured at positions on the outer sphere surface. These measurements were made on the system containing a 12-inch internal sphere. The center of the sphere was suspended about one meter above floor level to reduce neutron backscatter. The detector was a 5 mm-thick LiI(Eu) scintillation crystal with photomultiplier; counting was done with an RIDL scaler. Using the coordinate system shown in Figure C1, where the through-tube corresponds to the x-axis, measurements were taken by holding the azimuth angle θ constant at 0°, 45° and 90° and varying the colatitude; measurements were also made by holding the colatitude $\Phi = 67\text{-}1/2°$ and varying θ. These data are presented in graphical form in Figure C2.

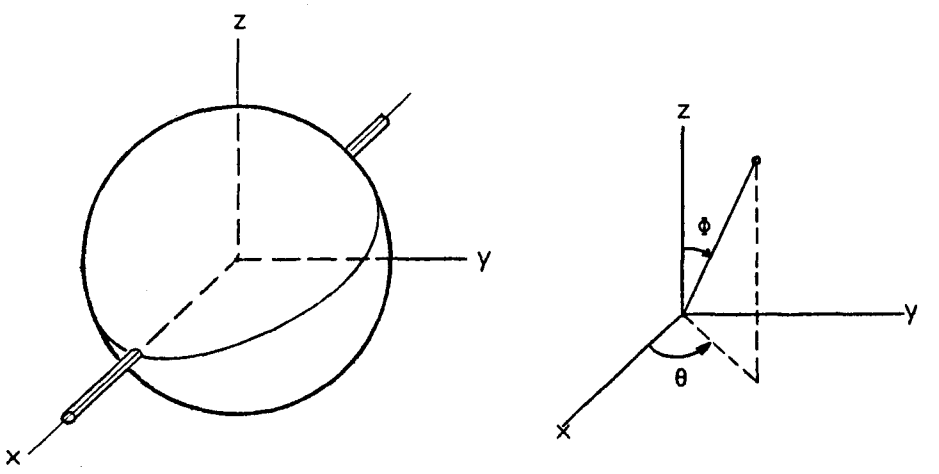

Figure C1. -- Coordinate system for measuring source asymmetry.

It was not possible to make a measurement for $\theta = 0°$ and $\Phi = 90°$ because of the presence of the through-tube, so extrapolation is necessary to establish this point on the graphs. Using this extrapolated value, it is seen that there is at least a 30 percent increase in source emission between this direction and $\theta = 90°$ with any Φ. As would be expected from source geometry, the source seems to be symmetric in the plane perpendicular to the through-tube.

Part of the asymmetry measured could be caused by the sphere being slightly out-of-round. However, measurements of the sphere dimensions indicate that any variance of the sphere radius is less than one centimeter, and probably much less. Since the sphere radius is 33.8 cm, the maximum change in count rate expected is thus $\frac{(33.8 + 1.0)^2}{(33.8)^2} = 1.06$, or a six percent change. Since a much greater change is observed in the count rates at different locations on the sphere surface, it must be concluded that most of the asymmetry observed in Figure C2 is due to asymmetry in the emission of the source and is not caused by the

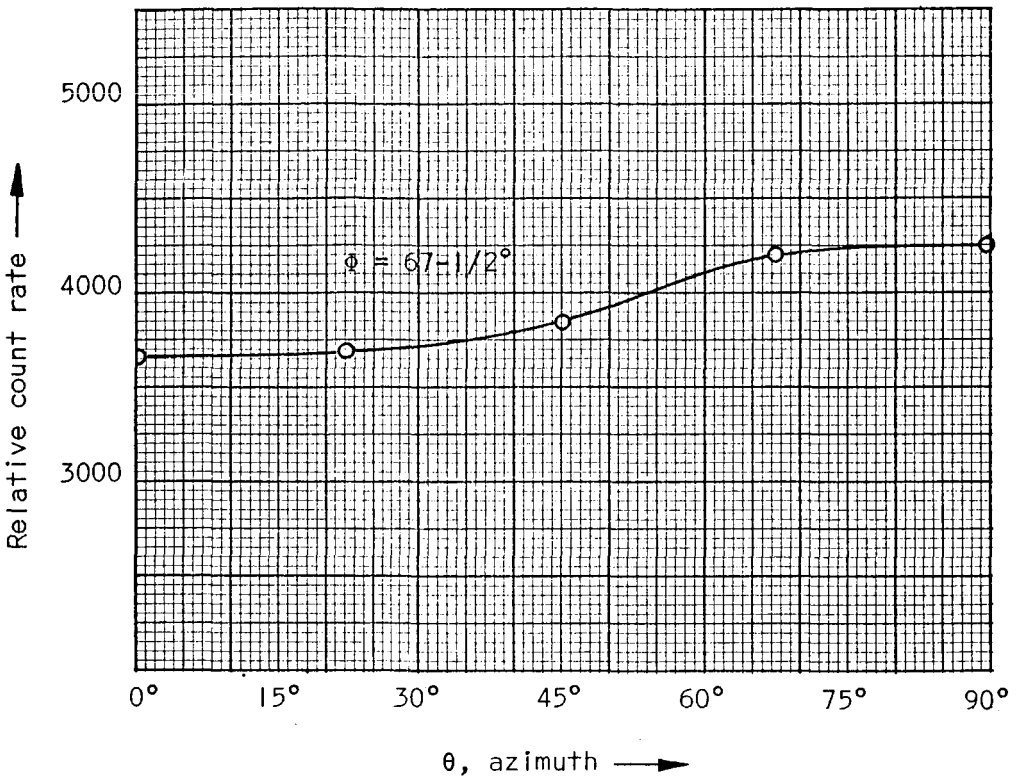

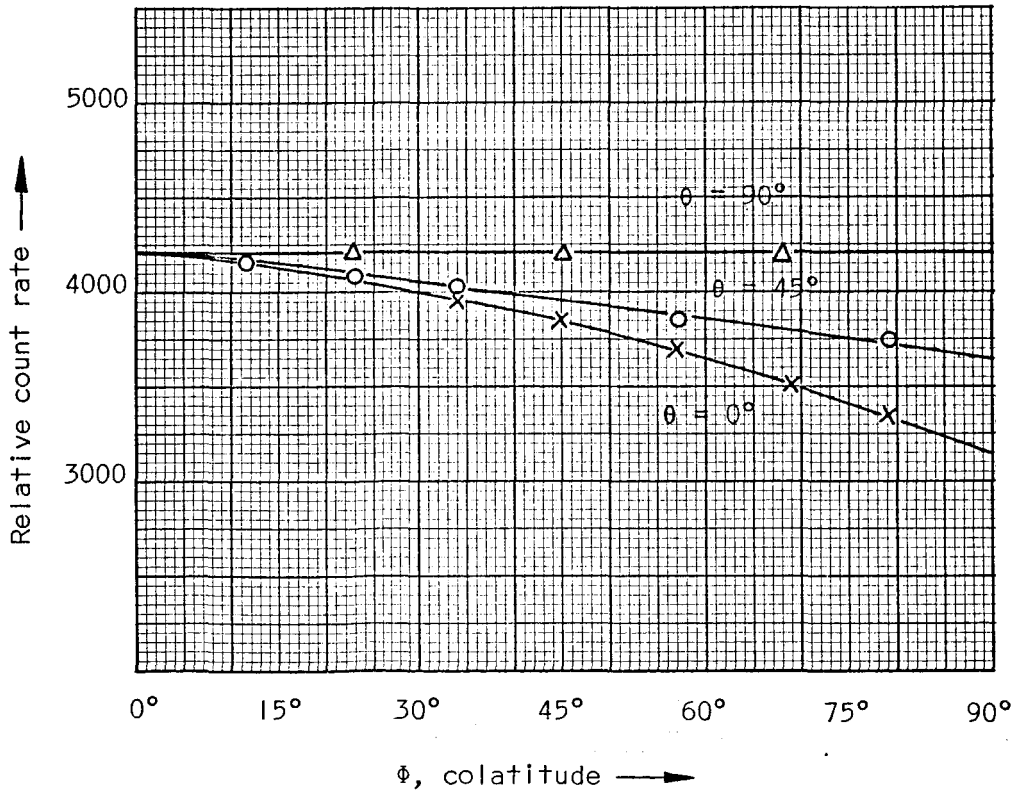

Figure C2. -- Change of fast neutron count rate as a function of azimuth and colatitude angles, showing the asymmetry of the Pu-Be source emission.

shape of the sphere.

During the experiments, it was first suspected that the emission of the source was not symmetric because foil activations measured at the same distance from the sphere surface but at different angles with respect to the source axis were different. They differed by a seemingly constant factor at any given radius at least an inch from the sphere surface. Activations anywhere on the sphere surface in the water agreed well with each other, however.

For a physical explanation of these two apparently contradictory facts, one should realize that the thermal neutron flux in water several mean free paths from any boundary is almost wholly dependent upon the fast flux at that point, and thus in this system it is proportional to the source emission in that direction. When there is little or no absorbing gas in the sphere, the thermal and epithermal neutrons in the water near the interface have been scattered back and forth through the sphere a number of times until their original locations are lost. Thus the flux inside the sphere and at the interface is probably nearly the same as the flux due to a symmetrically emitting source of the same average emission. When the absorption of the gas in the sphere is greater, fewer thermal neutrons pass through the sphere repeatedly, and so this 'smoothing out' of the interior fluxes could be expected to a lesser degree.

On the basis of the above discussion, it would be expected that the through-tube foil activations would show some sign of the source asymmetry, and that this would be more pronounced for the higher pres-

sures of BF_3 in the single sphere system. Since the through-tube foils are aligned along the axis of the source cylinder, and this happens to be the direction of minimum source emission, the foils there are likely to have a lower thermal activation near the interface. Nearer to the center of the sphere, neutrons will pass through the foils in relatively greater numbers from other parts of the sphere which present a greater source of thermal neutrons, so the activation would be greater there. This may be one explanation for the phenonenon of flux peaking toward the center of the sphere which was reported in reference 1. An investigation of the magnitude of these effects could be done experimentally, or it could be done theoretically with the use of two-dimensional spherical reactor codes.

Since the emission of the source is asymmetric, it can be expected that the experimental fluxes measured in the water are distorted near the interface. It is hard to say how one could relate the fluxes far out in the water with those measured in the sphere and on the surface. The simplest way would be to assume the measured fluxes inside the sphere were the same as those due to a symmetric source, and correct the fluxes far out in the water by the amount of asymmetry in the direction the foils were located. If the experiment were to be done over, the best way (in lieu of getting a truly symmetric source) would be to take experimental data only in those directions which have the same emission from the source as the source emission averaged over all angles.

It should be mentioned that while the data for reference 1 were

being taken a check was made to determine whether the flux was the same inside the sphere at locations other than the through-tube. This was done by attaching foil holders to caps which screwed into the outer sphere of the 9-inch and 12-inch inner sphere systems. However, for several reasons the asymmetry of the source was not observed. First, the counting procedure was not as accurate at that time as it has later become. It was further complicated by the fact that the water had to be drained from the tank to remove the foils, which resulted in a long delay time between the end of irradiation and the start of counting. Also, such a check was not possible in the single sphere system, which, with largest amounts of BF_3 , is the one which would be expected to show the effect of source asymmetry the most. Thus the data obtained at that time were not found to differ statistically from those measured in the through-tube.

NASA Lewis Research Center (2)
21000 Brookpark Road
Cleveland, Ohio 44135
Attention: Solomon Weiss (NTO)

NASA Lewis Research Center (1)
21000 Brookpark Road
Cleveland, Ohio 44135
Attention: Norman Musial

NASA Lewis Research Center (2)
21000 Brookpark Road
Cleveland, Ohio 44135
Attention: Library

NASA Lewis Research Center (6)
Lewis Technical Division
21000 Brookpark Road
Cleveland, Ohio 44135
Attention: Report Control Office

NASA Lewis Research Center (14)
21000 Brookpark Road
Cleveland, Ohio 44135
Attention: Robert Hyland

NASA Scientific and Technical Information Facility (6)
Box 5700
Bethesda, Maryland
Attention: NASA Representative

U.S. Atomic Energy Commission (3)
Technical Reports Library
Washington, D. C.

U.S. Atomic Energy Commission (3)
Technical Information Service Extension
P.O. Box 62
Oak Ridge, Tennessee

Mr. D. R. Bartz
Manager, Research & Advanced
Concepts Section
Propulsion Division
Jet Propulsion Laboratory
Pasadena, California 91103

Mr. J. R. Beyster
General Atomic
P. O. Box 608
San Diego, California 92115

Dr. Charles J. Bridgman
Associate Professor of Physics
Air Force Institute of Technology
Wright-Patterson Air Force Base, Ohio 45433

Mr. J. A. Brousseau
Chief, Propulsion Systems Technology
Mail Stop 47-18
The Boeing Company
Seattle, Washington 98124

Mr. James Carton
Advanced Concepts
REON Division
Aerojet-General Corporation
Sacramento, California 95801

Dr. C. C. Chang
Head, Space Sciences & Applied Physics
Catholic University
Washington, D. C. 20017

Dr. Peter Chiarulli
Head, Mechanics Department
Illinois Institute of Technology
Chicago, Illinois 60616

Mr. Holmes F. Crouch
Lockheed Missiles & Space Company
Space System Division
Department 62-90; Building 104
Sunnyvale, California 94408

Dr. Ralph S. Cooper
Chief Scientist
Donald W. Douglas Laboratories
P. O. Box 310
Richland, Washington 99352

Dr. Robert Dillaway
Nucleonics Department
Rocketdyne
6633 Canoga Avenue
Canoga Park, California 91303

Dr. D. W. Drawbaugh
Astronuclear Laboratory
Westinghouse Electric Corporation
Pittsburgh, Pennsylvania 15236

Mr. L. A. Gore
Space Technology Laboratories
One Space Park
Redondo Beach, California 90277

Professor Jerry Grey
Forrestal Research Center
Princeton University
Princeton, New Jersey 08540

Professor Robert A. Gross
School of Engineering &
Applied Science
Columbia University
New York, N. Y. 10027

Dr. A. V. Grosse
Research Institute of Temple Univ.
4150 Henry Avenue
Philadelphia, Pennsylvania 19144

Dr. George Grover
N-5
Los Alamos Scientific Laboratory
P. O. Box 1663
Los Alamos, New Mexico 87544

Dr. James W. Hadley
"R" Division Leader
Lawrence Radiation Laboratory
P. O. Box 808
Livermore, California 94551

Mr. L. P. Hatch
Brookhaven National Laboratory
Upton, Long Island, New York 11101

Dr. R. J. Holl
Missiles & Space Systems Division
Douglas Aircraft Company
Santa Monica, California 90405

Mr. J. W. Hilburn
Whiteshell Nuclear Research Establishment
Atomic Energy of Canada United
Pinawa, Manitoba,
Canada

Professor J. L. Kerrebrock
Room 33-115
Massachusetts Institute of Technology
Cambridge, Massachusetts 02139

Dr. John J. Keyes, Jr.
Reactor Division
Oak Ridge National Laboratory
P. O. Box Y
Oak Ridge, Tennessee 37831

Mr. Walter F. Krieve
Building S
TRW Systems
One Space Park
Redondo Beach, California 90278

Dr. W. S. Lewellyn
Manager, Fluid Dynamics Section
Aerospace Corporation
P. O. Box 95085
Los Angeles, California 90045

Mr. George H. McLafferty
United Aircraft Corporation
Research Laboratories
400 Main Street
East Hartford, Connecticut 06108

Professor Clyde Orr, Jr.
Chemical Engineering Department
Georgia Institute of Technology
Atlanta, Georgia 30301

Dr. Ben Pinkel
RAND Corporation
1700 Main Street
Santa Monica, California 90406

Dr. J. B. Romero
Advanced Nuclear Group
The Boeing Company
Seattle, Washington 98124

Dr. Richard Rosa
Avco Everett Research Laboratory
2385 Revere Beach Parkway
Everett, Massachusetts 02149

Dr. Martin Rosenzweig
Aerodynamic & Heat Transfer Dept.
Aerospace Corporation
P. O. Box 95085
Los Angeles, California 90045

Dr. S. M. Scala
Manager, Theoretical Fluid Physics Section
General Electric Company
Space Sciences Laboratory
P. O. Box 8555
Philadelphia, Pennsylvania 19101

Mr. W. L. Snapp
Aerojet-General Corporation
20545 Center Ridge Road
Cleveland, Ohio 44116

Dr. Robert F. Trapp
Chief, Advanced Concepts & Flight Projects (RBA)
Biotechnology and Human Research Division
National Aeronautics & Space Administration
Washington, D. C. 20546

Dr. Robert Uhrig
Chairman, Department of Nuclear Engineering
University of Florida
Gainesville, Florida 32601

Professor E. P. Wigner
Department of Physics
Princeton University
Princeton, New Jersey 08540

Captain William Yingling
AEC/NASA Space Nuclear Propulsion Office
Division of Reactor Development
U. S. Atomic Energy Commission
Washington, D. C. 20545

Mr. Jerrold M. Yos
Avco Corporation
Research & Advanced Development Division
201 Lowell Street
Wilmington, Massachusetts 01887

Professor M. J. Zucrow
Atkins Professor of Engineering
Mechanical Engineering Department
Purdue University
Lafayette, Indiana 47907